Journal of Robotics and Control (JRC)
Volume 3, Issue 3, May 2022
ISSN: 2715-5072 DOI: 10.18196/jrc.v3i3.14632

Dynamic Performance Analysis of a Five-Phase PMSM Drive Using Model Reference Adaptive System and Enhanced Sliding Mode Observer

Mahmoud A. Mossa [1*], Hamdi Echeikh [2], Alfian Ma'arif [3]
[1] Electrical Engineering Department, Faculty of Engineering, Minia University, Minia 61111, Egypt
[2] Department of Electrical Engineering, National Engineering School of Monastir, 5035, Tunisia
[3] Department of Electrical Engineering, Universitas Ahmad Dahlan, Yogyakarta 55191, Indonesia
Email: [1] mahmoud_a_mossa@mu.edu.eg, [2] hamdi.engineer.nl@gmail.com, [3] alfian.maarif@te.uad.ac.id
*Corresponding Author

***Abstract*—This paper aims to evaluate the dynamic performance of a five-phase PMSM drive using two different observers: sliding mode (SMO) and model reference adaptive system (MRAS). The design of the vector control for the drive is firstly introduced in details to visualize the proper selection of speed and current controllers' gains, then the construction of the two observers are presented. The stability check for the two observers are also presented and analyzed, and finally the evaluation results are presented to visualize the features of each sensorless technique and identify the advantages and shortages as well. The obtained results reveal that the designed SMO exhibits better performance and enhanced robustness compared with the MRAS under different operating conditions. This fact is approved through the obtained results considering a mismatch in the values of stator resistance and stator inductance as well. Large deviation in the values of estimated speed and rotor position are observed under MRAS, and this is also accompanied with high speed and torque oscillations.**

***Keywords*—Five phase PMSM; sensorless control; field orientation; current control; speed control; sliding mode; MRAS.**

Nomenclature	
SMO	Sliding mode observer
MRAS	Model reference adaptive system
PMSM	Permanent magnet synchronous motor
IM	Induction motor
EMF	Electromotive force
IRFOC	Indirect rotor field oriented control
LNN	Linear neural network
u_s, i_s, ψ_s	Stator voltage, stator current and stator flux
$\hat{\imath}_s$	Estimated stator current
$\tilde{\imath}_s$	Current estimation error
i_{max}	Nominal current
ψ_f	Rotor flux
R_s, L_s	Stator resistance and stator inductance
$\theta, \hat{\theta}$	Actual and estimated rotor positions
δ	Load angle
L_d,L_q, L_l	Direct, quadrature and leakage inductances
$\Omega^*, \Omega, \hat{\Omega}$	Reference, actual and estimated rotor speeds
Ω_{max}	Nominal speed
J_m	Motor inertia
B_m	Viscous friction
T_l,T_e	Load and developed torques
$K_{P\Omega}, K_{I\Omega}$	Coefficients of IP speed regulator
ω_n	Natural system frequency
ζ	Damping coefficient
t_{resp}	Speed response time
τ_i	Integral time constant
T_q	Time constant of current feedback loop
p	Pole pairs
z_d, z_q	Direct and quadrature current estimation errors
$K_{P\omega}, K_{I\omega}$	Coefficients of PI regulator used by MRAS

I. INTRODUCTION

For a number of years, multi-phase machines have found renewed interest [1-4]. In fact, the advances in power electronics enable providing suitable power supplies for these types of machines [5]. In addition, a large number of phases allows power segmentation which distributes the stresses on several components [6]. This allows, among other things, the use of power components operating with high switching frequency, and thus, reducing the harmonic content of the currents and the ripples of the torque [7]. Finally, these machines allow degraded running modes when a winding or a power component fails [8, 9]. However, these advantages should not overshadow the complexity of their order, both in normal and degraded modes [10, 11].

Permanent magnet synchronous motors have the following advantages over induction motors: A low inertia, which has the effect of giving a faster response for a given load change. A higher efficiency than that of conventional IMs, in fact the rotor joules losses are negligible for PMSM, while the rotor iron losses of an IM depend on the slip [12-14]. The PMSM does not require an excitation current source. For the same performance, the PMSM size is smaller; this advantage allows the use of PMSM machines where space is limited. However, the IM does not produce an expansion torque, which is the case with PMSM.

The most efficient controls such as "vector control" require precise knowledge of the rotor position. The encoders and resolvers provide this information. The presence of the sensors implies an increase in the volume, the overall cost of the system as well as a decrease in the reliability of the whole system. Moreover, it requires an available shaft end to add them, which is especially difficult for small machines [15]. In some cases, (motorization for naval propulsion), it is difficult or impossible to access it [16]. The industry continues searching to reduce the cost of implementation and

maintenance, to minimize the number of sensors. In the case where there are no speed and position sensors, it is therefore necessary to find a technique to estimate these quantities. Therefore, a solution is the use of observers. The observers known as "software sensors" which replace the mechanical sensors are a promising solution: observation and therefore control without a mechanical sensor becomes essential. In the literature there are several techniques for synthesizing a nonlinear observer for the synchronous permanent magnet machine. In general, these approaches can be classified into two categories: Approach based on high frequency signal injection and approach based on the machine model "fundamental excitation". The first is rather applied to anisotropic PMSM. The basic idea is to exploit the salience effect. This can be done by injecting additional high frequency excitation signal independent of the machine's fundamental power supply [17]. The second is to use a modified Pulse Width Modulation (PWM). The high frequencies used typically vary from 5 to 15 kHz [18, 19]. This means that the resistance will therefore be negligible while the current will depend mainly on the inductance. The rotor position will then be extracted from the measurement of the highfrequency current or voltage via signal processing. If the machine is with smooth poles, there is no saliency (inductances $L_d = L_q$). In this case, the salience of the magnetic saturation in the iron is low. This makes such technique sensitive to the converter non-linearities aswell as those of the magnetic circuit of the machine [20].

Signal injection techniques give better results at low speeds, including at standstill. On the other hand, they suffer from certain numbers of weaknesses, especially at high speed. They cause acoustic noise, ripples in the torque as well as additional iron losses which reduce the efficiency [21]. Consequently, solutions which combine high-frequency signal injection and the classical so-called "observer-hybrid" observation method have been proposed recently [22]. In other words, at low speed including at standstill, the method signal injection will be applied. Beyond that, classic observation will take over. A combination of an extended electromotive force (EEMF) observer (for further details) and signal injection is presented in [23]. A non-linear sliding mode observer was added to the signal injection in order to design a complete sensorless control [24].One is interested here in observation methods based on the machine model with regard to the secondapproach.

For PMSM with smooth pole, the majority of the work proposed is based on the estimation of electromotive forces (EMFs) from which position and speed are deduced [24, 25]. The estimation of EMFs can be classified into two categories depending on the reference plane from which the estimate is made. The second technique is to estimate these components in a hypothetical (virtual) rotating frame. If this coordinate system coincides with the synchronous coordinate system ($d-q$), the direct component of EMF becomes zero [26]. This introduces a very strong criterion which makes it possible to correct the position and the speed of the hypothetical reference frame so that it synchronizes with the rotating frame (d-q) linked to the rotor. Consequently, the position and the speed of the rotor are deduced directly from the position and the speed of the hypothetical frame. On the other hand, this method is not suitable for anisotropic PMSM ($L_d \neq L_q$), where the position information is contained not only in the EMF, but also in the inductances.

Consequently, the concept of extended EMFs has been developed either in a hypothetical frame mentioned above [27] or in a fixed frame ($\alpha-\beta$) [28]. Estimating the flux also helps in determining the speed and position of the rotor. An EMF estimator has been presented in [29] to estimate position as well as speed. This pattern is sensitive to noise and also to change in resistance. An observer to estimate the rotor flux has been developed [30]. In [31] and [32] observers based on the extended Kalman filter (EKF) were used. Although these filters are stable and well known, they involve a significant computation cost and require a very precise initialization. On the other hand, [33] developed a discrete extended Kalman filter. The algorithm used had the advantage of reducing the calculation cost (-3.6%) compared to a conventional filter.

The study in [34] proposed another more efficient observer, called a two-level Kalman filter. The two-level Kalman filtering allows a significant reduction in the computation cost (-21%) while retaining the performance of conventional EKF. Artificial neural networks integrate the estimation of the mechanical quantities of PMSM. In [35], an observer based on this technique is proposed. Similarly, in [36], an observer based on the same technique was applied to the PMSM. The latter estimates the position while the speed is assumed to be known. In addition, adaptive observers are presented in [37, 38]. High gain interconnected observers have been developed in [39-43], and defined in the fixed coordinate system ($\alpha-\beta$) for the application of the wind turbine. In addition, the adaptive reference model method has been studied in [44, 45]. In this last paper, it is shown that the simultaneous estimation of the stator resistance and the rotor flux is not possible.

Recently multi-phase machines attracted the interests of many researchers due to their advantages of fault tolerant capability and increased torque density compared with the three phase types, but there are no extensive works considering the observers applied for speed and rotor position identification. In [46], a sensorless control under open phase fault condition is presented using the estimation of the Five-phase IM speed using the MRAS observer. An estimation approach is proposed in [47] to determinate the motor parameters being the stator and rotor resistances and the magnetizing inductance of a five-phase IM. A sensorless vector control for a five-phase PMSM drive is demonstrated in [48], this method is based on the EMF estimation from which the speed and position are extracted. In [49] a new construction of an adaptive SMO is developed; this paper uses an online determination of the rotor resistance of five-phase IM in order to eliminate the effects of the resistance variation. A sensorless vector controlled base EKF of two five phase IM series-connected with a control of the current in the stationary reference frame is introduced in [50]. An MRAS-based sensorless IRFOC of five-phase IM is also presented in [51]. In [52], a sensorless scheme is proposed based on the utilization of back EMF in addition to an

adaptive band-pass filter in order to estimate the rotor position of a field oriented controlled five phase PMSM. This technique requires precise determination of the band pass frequency under different operating speeds. In [53] and [54], an extended kalman filter (EKF) was utilized to observe the rotor position and speed of a five phase PMSM under sliding mode control regime. The main shortage in theses technique was the system complexity and the need for identifying the covariance and gain matrices. In [55], a second order integrator with a frequency locked loop (FLL) is utilized to estimate the rotor position for a five phase PMSM under FOC.

However, the main drawback in this technique is the sensitivity of the FLL to disturbances. In [56], an unknown input observer is utilized for a backstepping controlled five phase PMSM in order to solve the problem of speed sensor fault. In [57], an adaptive scheme based on a linear neural network (LNN) is utilized to estimate the position of a five phase PMSM. The learning rule of LNN is based on the least mean square principle, which is a very primitive learning rule that cannot satisfy the proper operation of the LNN in different operating frequencies. In [58], a rotor position estimator is introduced utilizing the voltage model of the five-phase PMSM represented in two frames: the rotor reference frame and another virtual frame. The main drawback of this technique is the sensitivity to model uncertainties.

As an attempt to investigate more about the convenient estimators used for five phase PMSM and presenting a detailed analysis for their performances, this paper deals with presenting two different observers approaches for the five-phase PMSM drive. The two sensorless approaches are the SMO and MRAS observers. The designed SMO utilizes the saturation function instead of using the signum function, which is generally used in classic SMO. The saturation function inherently smooths the estimated back-emf signal without the need to use low-pass filters (LPF) as adopted with classic SMO. Usually LPFs are used to attenuate the discontinuous switching signals. The stability analysis of both methods is developed. A detailed comparison between the two methods in different range of speed and especially at low speed operation is presented. The simulation results are presented to show the performances and the effectiveness of both methods. Weakness points are also addressed. This is to introduce a detailed view about the mechanism by which each observer is working, and when it works properly as well as when it fails in the estimation task.

The contributions that the present study introduces to the literature can be outlined as following

- The paper presents the detailed design of two sensorless techniques for a five-phase PMSM drive.
- The control system is systematically designed and combined with the sensorless schemes for the proper operation of the five-phase PMSM drive.
- A comprehensive performance analysis for the two sensorless schemes under different operating frequencies is introduced.
- The stability analysis for both observation techniques are introduced and explained.
- The capability of the two estimators under uncertainties and system disturbances is investigated to visualize the most efficient observer.

The paper is formulated as follows: Sec. II reports a detailed presentation of the five-phase PMSM motor, all the mathematical models in the reference frame (α-β-z-w) and the rotating frame (d-q-x-y) are introduced. Sec. III presents the detailed design of the vector control system. In Sec. IV, a design of sliding mode observer in order to estimate both the motor speed and the mechanical position is described; also a stability analysis of the proposed method is demonstrated. Secs. V and VI present a comprehensive study of the MRAS system to estimate the speed and mechanical position and followed by a stability analysis demonstration. Simulation results and discussion for the two observers for the vector controlled drive are illustrated in Secs. VII and VIII. Finally, Sec. IX reports the conclusions disclosed to contributions given in the paper.

II. MODELING OF FIVE PHASE PMSM

The mathematical model of the motor in stationary ($\alpha-\beta$) and the rotating ($d-q$) reference frames can be obtained in the following procedure. The stator voltage equations are

$$u_s = R_s i_s + \frac{d\psi_s}{dt} \tag{1}$$

where the air-gap flux linkages are introduced by

$$\psi_s = \psi_{ss} + \psi_f = L_s i_s + \psi_f \tag{2}$$

where $u_s = [u_{sa} \quad u_{sb} \quad u_{sc} \quad u_{se} \quad u_{sf}]^T$, and $i_s = [i_{sa} \quad i_{sb} \quad i_{sc} \quad i_{se} \quad i_{sf}]^T$ are the stator voltage and current vectors, respectively.

Then, $R_s = diag[R_s \quad R_s \quad R_s \quad R_s \quad R_s]$.

$$L_s = L_l I + L_m M \tag{3}$$

$$I = \begin{bmatrix} 1 & 0 & 0 & 0 & 0 \\ 0 & 1 & 0 & 0 & 0 \\ 0 & 0 & 1 & 0 & 0 \\ 0 & 0 & 0 & 1 & 0 \\ 0 & 0 & 0 & 0 & 1 \end{bmatrix}, \psi_f = |\psi_f| \begin{bmatrix} \cos\theta \\ \cos(\theta - \delta) \\ \cos(\theta - 2\delta) \\ \cos(\theta - 3\delta) \\ \cos(\theta - 4\delta) \end{bmatrix} \tag{4}$$

$$M = \begin{bmatrix} 1 & \cos\delta & \cos 2\delta & \cos 3\delta & \cos 4\delta \\ \cos 4\delta & 1 & \cos\delta & \cos 2\delta & \cos 3\delta \\ \cos 3\delta & \cos 4\delta & 1 & \cos\delta & \cos 2\delta \\ \cos 2\delta & \cos 3\delta & \cos 4\delta & 1 & \cos\delta \\ \cos\delta & \cos 2\delta & \cos 3\delta & \cos 4\delta & 1 \end{bmatrix} \tag{5}$$

In equation (4) and equation (5), δ is equal to $2\pi/5$ and denotes the angle of the stator coil spatial position, L_m is the main inductance, θ is the electrical angle of the rotor, L_l is the stator leakage inductance, $|\psi_f|$ is the permanent magnet flux amplitude.

Utilizing the winding function procedure, the winding inductance matrix can be obtained which is position dependent. A coordinate transformation is established for facilitating the model, which transfers the variables of five-phase PMSM into a rotating reference frame. For this system, the transformation matrix $T(\theta)$ can be formulated as shown in (6):

$$T(\theta) = \frac{2}{5}\begin{bmatrix} \cos\theta & \cos\left(\theta-\frac{2\pi}{5}\right) & \cos\left(\theta-\frac{4\pi}{5}\right) & \cos\left(\theta-\frac{6\pi}{5}\right) & \cos\left(\theta-\frac{8\pi}{5}\right) \\ \sin\theta & \sin\left(\theta-\frac{2\pi}{5}\right) & \sin\left(\theta-\frac{4\pi}{5}\right) & \sin\left(\theta-\frac{6\pi}{5}\right) & \sin\left(\theta-\frac{8\pi}{5}\right) \\ \cos\theta & \cos\left(\theta-\frac{4\pi}{5}\right) & \cos\left(\theta-\frac{8\pi}{5}\right) & \cos\left(\theta-\frac{2\pi}{5}\right) & \cos\left(\theta-\frac{6\pi}{5}\right) \\ \sin\theta & \sin\left(\theta-\frac{4\pi}{5}\right) & \sin\left(\theta-\frac{8\pi}{5}\right) & \sin\left(\theta-\frac{2\pi}{5}\right) & \sin\left(\theta-\frac{6\pi}{5}\right) \\ \frac{1}{2} & \frac{1}{2} & \frac{1}{2} & \frac{1}{2} & \frac{1}{2} \end{bmatrix} \quad (6)$$

This transformation matrix is characterized with the pseudo orthogonal property.

$$T^{-1}(\theta) = \frac{5}{2}T^{T}(\theta) \quad (7)$$

where $T^{T}(\theta)$ and $T^{-1}(\theta)$ are the transpose and inverse matrices of $T(\theta)$, respectively. The co-ordinate systems exploited for this paper presented in [51]. (d-q) is the rotor flux reference frame, (α-β) is the stationary two-phase reference frame and (x-y) is the stator leakage flux reference frame. δ is the load angle between the rotor and stator flux linkages where δ is constant during the steady states for a specific load torque, meanwhile it varies during transients, and the rotational speed of the rotor and stator fluxes is dissimilar. By implementing the previously noted transformation to the rotor and stator voltages and the flux-linkage and torque, the following equations are obtained in the synchronous rotating reference frame (d- q- x- y-o). The stator flux linkages are given by

$$\begin{cases} \psi_{sd} = L_d i_{sd} + \psi_f \\ \psi_{sq} = L_q i_{sq} \\ \psi_{sx} = L_l i_{sx} \\ \psi_{sy} = L_l i_{sy} \\ \psi_{so} = L_l i_{so} \end{cases} \quad (8)$$

where $L_d = L_l + L_{md}$ and $L_q = L_l + L_{mq}$.

An illustration of the transformed flux components using the transformation matrices is illustrated in Fig. 1. The stator voltages in (d- q- x- y-o) are given by

$$\begin{cases} u_{sd} = R_s i_{sd} + \frac{d\psi_{sd}}{dt} - \omega\psi_{sq} \\ u_{sq} = R_s i_{sq} + \frac{d\psi_{sq}}{dt} + \omega\psi_{sd} \\ u_{sx} = R_s i_{sx} + \frac{d\psi_{sx}}{dt} \\ u_{sy} = R_s i_{sy} + \frac{d\psi_{sy}}{dt} \\ u_{so} = R_s i_{so} + \frac{d\psi_{so}}{dt} \end{cases} \quad (9)$$

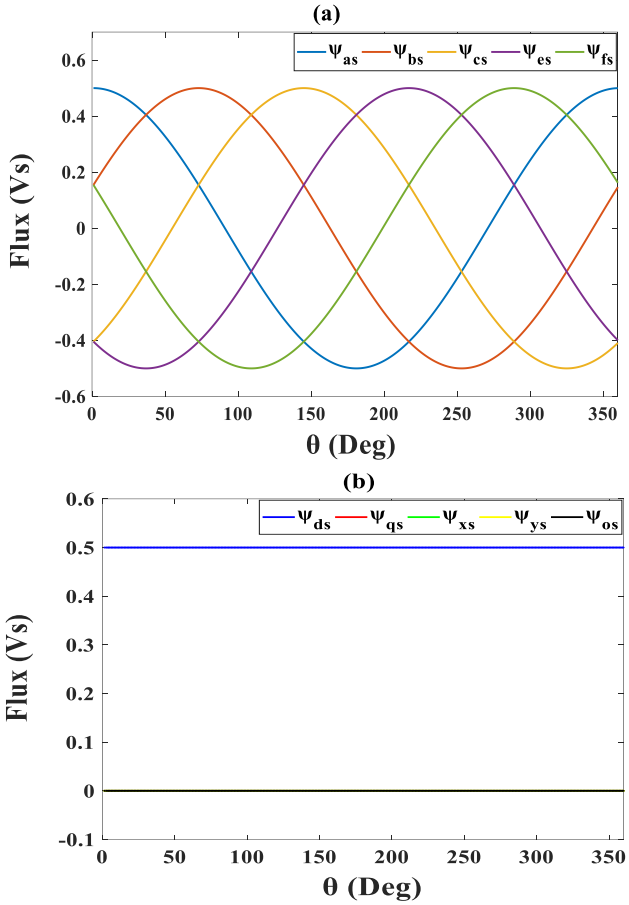

Fig. 1. Flux profiles: (a) ψ_{sabcef} , (b) ψ_{sdqxyo}

The torque can be calculated by

$$T_e = \frac{5}{2}p[\psi_f i_{sq} + (L_d - L_q)i_{sq}i_{sd}] \quad (10)$$

The torque can be expressed also as

$$T_e = \frac{5}{2}p[\psi_{sd} i_{sq} - \psi_{sq} i_{sd}] \quad (11)$$

From (8) and (9), the dynamic model of the FPMSM can be represented in the rotating frame by

$$\begin{cases} \frac{di_{sd}}{dt} = \frac{1}{L_d}u_{sd} - \frac{R_s}{L_d}i_{sd} + p\frac{L_q}{L_d}\Omega i_{sq} \\ \frac{di_{sq}}{dt} = \frac{1}{L_q}u_{sq} - \frac{R_s}{L_q}i_{sq} - p\frac{L_d}{L_q}\Omega i_{sd} - p\frac{\psi_f}{L_q}\Omega \\ \frac{di_{sx}}{dt} = \frac{1}{L_l}u_{sx} - \frac{R_s}{L_l}i_{sx} \\ \frac{di_{sy}}{dt} = \frac{1}{L_l}u_{sy} - \frac{R_s}{L_l}i_{sy} \\ T_e = \frac{5}{2}p[\psi_f i_{sq} + (L_d - L_q)i_{sq}i_{sd}] \\ J_m\frac{d\Omega}{dt} = T_e - T_L - B_m\Omega \end{cases} \quad (12)$$

Where Ω is the mechanical speed, J_m is the motor inertia, B_m is the viscous friction and T_L is the load torque.

The general system in the reference frame (*α-β-z-w-o*) of the five-phase PMSM can be also obtained as follows

$$\begin{cases} \dfrac{di_{s\alpha}}{dt} = \dfrac{1}{L_{s\alpha}}u_{s\alpha} - \dfrac{R_s}{L_{s\alpha}}i_{s\alpha} + \dfrac{p\psi_f}{L_{s\alpha}}\Omega\sin\theta \\ \dfrac{di_{s\beta}}{dt} = \dfrac{1}{L_{s\beta}}u_{s\beta} - \dfrac{R_s}{L_{s\beta}}i_{s\beta} - \dfrac{p\psi_f}{L_{s\beta}}\Omega\cos\theta \\ \dfrac{di_{sz}}{dt} = \dfrac{1}{L_l}u_{sz} - \dfrac{R_s}{L_l}i_{sz} \\ \dfrac{di_{sw}}{dt} = \dfrac{1}{L_l}u_{sw} - \dfrac{R_s}{L_l}i_{sw} \\ T_e = \dfrac{5}{2}p\psi_f[i_{s\beta}\cos\theta - i_{s\alpha}\sin\theta] \\ J_m\dfrac{d\Omega}{dt} = T_e - T_L - B_m\Omega \end{cases} \quad (13)$$

The dynamic model in (13) will be used to construct the SMO for the five phase PMSM as presented in Sec. 4. The typical isolated neutral five-leg inverter structure is utilized to drive the five-phase PMSM, as shown in Fig. 2.

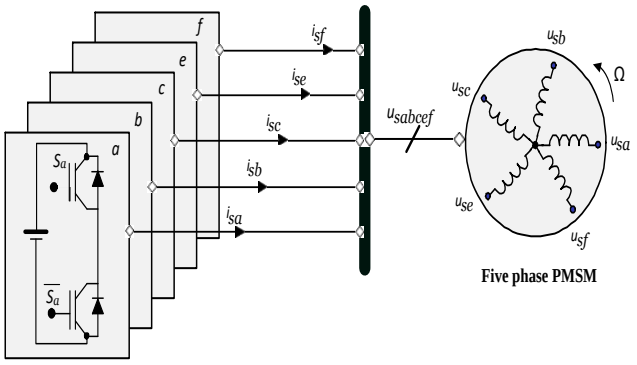

Fig. 2. Schematic diagram of the five-phase PMSM drive system

III. CONTROL SYSTEM DESIGN

Under vector control considering an isotropic machine ($L_d = L_q$), the stator current component i_{sq} manages the torque production, whereas the current components i_{sd}, i_{sx} and i_{sy} are maintained at zero. In addition, typical decoupling is applied.

The design of speed control loop is accomplished using an IP regulator; meanwhile the current control loop is constructed using a PI regulator. The outputs of the PI regulators are then summed to the decouple parts to finally formulate the voltage references. The tuning process of both regulators is accomplished systematically in the following subsections.

3.1. Design of speed regulator

The schematic of the closed-loop of speed regulation is illustrated in Fig. 3, in which it is shown that an IP regulator is utilized for the regulation purpose. The coefficients of the IP controllers ($K_{P\Omega}$, $K_{I\Omega}$) are synthesized as following.

From Fig. 3, the transfer function of the speed control loop can be expressed by

$$H = \frac{\hat{\Omega}}{\Omega^*} = \frac{1}{\dfrac{J_m}{K_{P\Omega}\,K_{I\Omega}}s^2 + \dfrac{(J_m + K_{P\Omega})}{K_{P\Omega}\,K_{I\Omega}}s + 1} \quad (14)$$

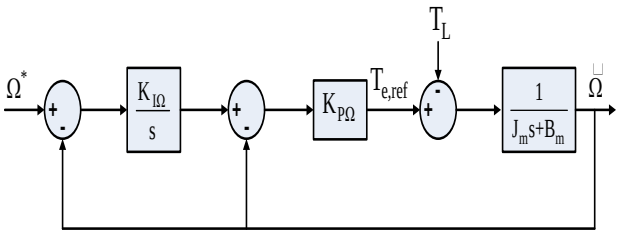

Fig. 3. Schematic diagram of speed control loop

The second-order dynamic of transfer function can be also expressed by

$$H = \frac{1}{\dfrac{1}{\omega_n^2}s^2 + \dfrac{2\zeta}{\omega_n}s + 1} \quad (15)$$

Where ω_n and ζ are the natural system frequency and damping coefficient, respectively.

By comparing (16) and (17), it results

$$\frac{J_m}{K_{P\Omega}\,K_{I\Omega}} = \frac{1}{\omega_n^2}$$

and (16)

$$\frac{(J_m + K_{P\Omega})}{K_{P\Omega}\,K_{I\Omega}} = \frac{2\zeta}{\omega_n}$$

The coefficient ζ is selected as 0.7, corresponding to a value of $\omega_n t_{resp} = 3$ as given in Table 1, where t_{resp} is the speed response time.

TABLE I. RELEVANT VALUES BETWEEN ζ AND $\omega_n t_{resp}$

ζ	$\omega_n t_{resp}$
0.4	7.7
0.5	5.3
0.6	5.2
0.7	3
1	4.75

Consequently, the parameters of the speed controller are identified by

$$K_{P\Omega} = 2J_m\omega_n - B_m$$

and (17)

$$K_{I\Omega} = \frac{J_m\omega_n^2}{(2J_m\omega_n - B_m)}$$

3.1. Design of current regulators

In this stage, the (*d*, *q*, *x*, *y*) current component control loops are structured and PI regulators are used for this purpose. These controllers are responsible for generating the active reference voltages, which are then added to the compensating terms to formulate finally the reference voltages. As the current loops for the *d* and *q* components and are similar; the same as *x* and *y* components, thus only

two control loops for the *q* and *x* current components are designed which are providing the same function for the *d* and *y* current components, respectively.

Figs. 4 and 5 show the schematic diagram of closed-loop current controllers for the *q* and *x* axes, respectively.

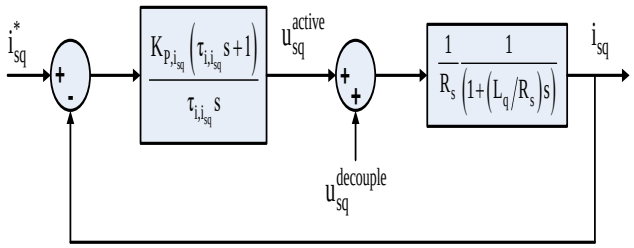

Fig. 4. Schematic diagram of q-axis current control loop

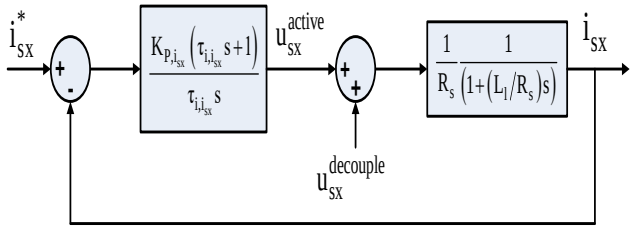

Fig. 5. Schematic diagram of x-axis current control loop

The control loops of the *d-q* axes current components have the same integral time-constant $\tau_{i,i_{sq}}$ and proportional factor $K_{P,i_{sq}}$. Meanwhile, the *x-y* current loops have a similar integral time-constant $\tau_{i,i_{sx}}$ and proportional factor $K_{P,i_{sx}}$.

Consequently, the transfer functions of the PI regulators for the *d-q* and *x-y* current control loops are given respectively by

$$\frac{K_{P,i_{sq}}\left(\tau_{i,i_{sq}}s+1\right)}{\tau_{i,i_{sq}}s} \quad \text{and} \quad \frac{K_{P,i_{sx}}\left(\tau_{i,i_{sx}}s+1\right)}{\tau_{i,i_{sx}}s} \tag{18}$$

The PI parameters selection is performed according to two bases:

i. The pole of the system is cancelled by the zero of the current regulator.
ii. The feedback loop time constant is selected to be lower than that of the system.

In Fig. 3, the closed loop system function of the *q*-current is expressed by

$$H_{ol,i_{sq}}=\frac{K_{P,i_{sq}}\left(\tau_{i,i_{sq}}s+1\right)}{\tau_{i,i_{sq}}s}\frac{1}{R_s}\frac{1}{\left(1+\left(L_q/R_s\right)s\right)} \tag{19}$$

where $\left(L_q/R_s\right)$ is the time-coefficient of the *d-q* currents loop.

By considering that

$$\tau_{i,i_{sq}}s+1=1+\left(L_q/R_s\right)s \tag{20}$$

This results in simplifying (19) to be

$$H_{ol,i_{sq}}=\frac{1}{R_s\left(\tau_{i,i_{sq}}/K_{P,i_{sq}}\right)s}=\frac{1}{T_q s} \tag{21}$$

where T_q is the time-constant of the current feedback loop, which can be defined as given in [59] by

$$T_q=R_s\frac{\tau_{i,i_{sq}}}{K_{P,i_{sq}}}=0.116\frac{L_q}{R_s} \tag{22}$$

By manipulating (22) and (20), the proportional constant $K_{P,i_{sq}}$ and integral time constant $\tau_{i,i_{sq}}$ can be obtained as follows

$$K_{P,i_{sq}}=\frac{R_s}{0.116} \quad \text{and} \quad \tau_{i,i_{sq}}=\frac{L_q}{R_s} \tag{23}$$

For the current loop of *x*-axis current illustrated in Fig. 5, the open loop system function can be evaluated by

$$H_{ol,i_{sx}}=\frac{K_{P,i_{sx}}\left(\tau_{i,i_{sx}}s+1\right)}{\tau_{i,i_{sx}}s}\frac{1}{R_s}\frac{1}{(1+(L_l/R_s)s)} \tag{24}$$

The first rule of the loop system function can be represented by

$$\tau_{i,i_{sx}}s+1=1+(L_l/R_s)s \tag{25}$$

Then, (24) can be simplified by

$$H_{ol,i_{sx}}=\frac{1}{1+R_s\left(\tau_{i,i_{sx}}/K_{P,i_{sx}}\right)s}=\frac{1}{1+T_x s} \tag{26}$$

where

$$T_x=R_s\frac{\tau_{i,i_{sx}}}{K_{P,i_{sx}}}=0.116\frac{L_l}{R_s}.$$

Then, the coefficients of the regulator are calculated by

$$K_{P,i_{sx}}=\frac{R_s}{0.116} \quad \text{and} \quad \tau_{i,i_{sx}}=\frac{L_l}{R_s} \tag{27}$$

IV. DESIGN OF SMO FOR FIVE PHASE PMSM

Among the different observation methods used, for their robustness qualities, sliding mode observers (SMOs) have been widely studied in order to estimate unmeasured

mechanical quantities for different types of machine drives. SMOs have private features, in that the capability to develop a sliding motion on the deviation among the measured plant outrun and the outrun of the estimator ensures that a SMO develops a series of state-estimates that are accurately correlative to the real plant output. However, the extensive utilization of SMO with different types of machine drives, but one cannot find a plenty of literature work about the design of SMO for the five-phase PMSM drives.

Generally, in classic SMO observers which utilize the *signum* function; in order to guarantee a correct sliding mode, an infinite switching frequency is required [60, 61], which cannot be afforded in real implementation. In addition, the chattering phenomenon is another challenge which requires using a low-pass filter (LPF) to smooth the discontinuous switching signals [62].

To avoid the shortages of *signum* function based SMO, this section is dedicated to introduce a systematic design of an effective SMO for the five-phase PMSM. The designed SMO utilizes the saturation (*sat*) function as an alternative to the *signum*, taking the advantage of *sat* function in its ability to smooth the estimated signals without using LPFs.

The SMO for the five-phase PMSM can be described using the following formulations

$$\begin{cases} \dfrac{d\hat{\imath}_{s\alpha}}{dt} = \dfrac{1}{L_{s\alpha}}u_{s\alpha} - \dfrac{R_s}{L_{s\alpha}}\hat{\imath}_{s\alpha} + p\hat{\Omega}\dfrac{\psi_f}{L_{s\alpha}}\sin\hat{\theta} + K_{\alpha\beta}.sat(\tilde{\imath}_{s\alpha}) \\ \dfrac{d\hat{\imath}_{s\beta}}{dt} = \dfrac{1}{L_{s\beta}}u_{s\beta} - \dfrac{R_s}{L_{s\beta}}\hat{\imath}_{s\beta} - p\hat{\Omega}\dfrac{\psi_f}{L_{s\beta}}\cos\hat{\theta} + K_{\alpha\beta}.sat(\tilde{\imath}_{s\beta}) \\ \dfrac{d\hat{\imath}_{sz}}{dt} = \dfrac{1}{L_l}u_{sz} - \dfrac{R_s}{L_l}\hat{\imath}_{sz} + K_{zw}.sat(\tilde{\imath}_{sz}) \\ \dfrac{d\hat{\imath}_{sw}}{dt} = \dfrac{1}{L_l}u_{sw} - \dfrac{R_s}{L_l}\hat{\imath}_{sw} + K_{zw}.sat(\tilde{\imath}_{sw}) \\ \dfrac{d\hat{\Omega}}{dt} = \dfrac{5}{2}\dfrac{p\psi_f}{J_m}\left(\hat{\imath}_{s\beta}\cos\hat{\theta} - \dot{\hat{\imath}}_{s\alpha}\sin\hat{\theta}\right) - \dfrac{B_m}{J_m}\hat{\Omega} + K_{\Omega}.sat(\tilde{\imath}_{s\alpha}) + K_{\Omega}.sat(\tilde{\imath}_{s\beta}) \\ \dfrac{d\hat{\theta}}{dt} = \hat{\Omega} + K_{\theta}.sat(\tilde{\imath}_{s\alpha}) + K_{\theta}.sat(\tilde{\imath}_{s\beta}) \end{cases} \tag{28}$$

where $\tilde{\imath}_{s\alpha} = i_{s\alpha} - \hat{\imath}_{s\alpha}$, $\tilde{\imath}_{s\beta} = i_{s\beta} - \hat{\imath}_{s\beta}$, $\tilde{\imath}_{sz} = i_{sz} - \hat{\imath}_{sz}$, and $\tilde{\imath}_{sw} = i_{sw} - \hat{\imath}_{sw}$ design the current estimation errors and the observer gains are presented with $K_{\alpha\beta}$, K_{zw}, K_{Ω} and K_{θ}. Consequently, this yields to the dynamics of the estimation errors to be expressed by

$$\begin{aligned} \frac{d\tilde{\imath}_{s\alpha}}{dt} &= -\frac{R_s}{L_{s\alpha}}\tilde{\imath}_{s\alpha} + p\frac{\psi_f}{L_{s\alpha}}\left(\Omega\sin\theta - \hat{\Omega}\sin\hat{\theta}\right) - K_{\alpha\beta}.sat(\tilde{\imath}_{s\alpha}) \\ \frac{d\tilde{\imath}_{s\beta}}{dt} &= -\frac{R_s}{L_{s\beta}}\tilde{\imath}_{s\beta} + p\frac{\psi_f}{L_{s\beta}}\left(\hat{\Omega}\cos\hat{\theta} - \Omega\cos\theta\right) - K_{\alpha\beta}.sat(\tilde{\imath}_{s\beta}) \\ \frac{d\tilde{\imath}_{sz}}{dt} &= -\frac{R_s}{L_l}\tilde{\imath}_{sz} - K_{zw}.sat(\tilde{\imath}_{sz}) \\ \frac{d\tilde{\imath}_{sw}}{dt} &= -\frac{R_s}{L_l}\tilde{\imath}_{sw} - K_{zw}.sat(\tilde{\imath}_{sw}) \end{aligned}$$

$$\begin{aligned} \frac{d\tilde{\Omega}}{dt} &= \frac{5}{2}\frac{p\psi_f}{J_m}\left[\left(i_{s\beta}\cos\theta - i_{s\alpha}\sin\theta\right) - \left(\hat{\imath}_{s\beta}\cos\hat{\theta} - \hat{\imath}_{s\alpha}\sin\hat{\theta}\right)\right] \\ &\quad - \frac{B_m}{J_m}\tilde{\Omega} - K_{\Omega}.sat(\tilde{\imath}_{s\alpha}) - K_{\Omega}.sat(\tilde{\imath}_{s\beta}) \\ \frac{d\tilde{\theta}}{dt} &= \Omega - \hat{\Omega} - K_{\theta}.sat(\tilde{\imath}_{s\alpha}) - K_{\theta}.sat(\tilde{\imath}_{s\beta}) \end{aligned} \tag{29}$$

Where $\tilde{\Omega} = \Omega - \hat{\Omega}$ and $\tilde{\theta} = \theta - \hat{\theta}$ design respectively the dynamics estimation errors of the mechanical speed and the rotor angular position. After that, one can use the Lyapunov's candidate function to prove the observer convergence as follows

$$V = \frac{1}{2}\left(\tilde{\imath}_{s\alpha}^2 + \tilde{\imath}_{s\beta}^2 + \tilde{\imath}_{sz}^2 + \tilde{\imath}_{sw}^2 + \tilde{\Omega}^2 + \tilde{\theta}^2\right) \tag{30}$$

Its time derivative presented as

$$\dot{V} = \tilde{\imath}_{s\alpha}\dot{\tilde{\imath}}_{s\alpha} + \tilde{\imath}_{s\beta}\dot{\tilde{\imath}}_{s\beta} + \tilde{\imath}_{sz}\dot{\tilde{\imath}}_{sz} + \tilde{\imath}_{sw}\dot{\tilde{\imath}}_{sw} + \tilde{\Omega}\dot{\tilde{\Omega}} + \tilde{\theta}\dot{\tilde{\theta}} \tag{31}$$

Lyapunov formulas are used in different aspects (convergence check, stability check, design of MRAS systems, etc.). The Lyapunov technique is articulated on the physical idea that an isolated system loses gradually its stored energy by time. A Lyapunov function maps vector or scalar variables to real numbers $\left(R^{\bar{N}} \to R_+\right)$ and reduces with time. The simplicity of the Lyapunov technique is the main feature which makes it valid for treating several engineering problems. The main challenge to apply the Lyapunov methodology is in finding an appropriate Lyapunov function. In the following sections, we consider that for the considered problem, the Lyapunov function (30) is a proper function. Equation (31) is rewritten as

$$\begin{aligned} \dot{V} = {} & \tilde{\imath}_{s\alpha}\left[-\frac{R_s}{L_{s\alpha}}\tilde{\imath}_{s\alpha} + p\frac{\psi_f}{L_{s\alpha}}\left(\Omega\sin\theta - \hat{\Omega}\sin\hat{\theta}\right) - K_{\alpha\beta}.sat(\tilde{\imath}_{s\alpha})\right] \\ & + \tilde{\imath}_{s\beta}\left[-\frac{R_s}{L_{s\beta}}\tilde{\imath}_{s\beta} + p\frac{\psi_f}{L_{s\beta}}\left(\hat{\Omega}\cos\hat{\theta} - \Omega\cos\theta\right) - K_{\alpha\beta}.sat(\tilde{\imath}_{s\beta})\right] \\ & + \tilde{\imath}_{sz}\left[-\frac{R_s}{L_l}\tilde{\imath}_{sz} - K_{zw}.sat(\tilde{\imath}_{sz})\right] \\ & + \tilde{\imath}_{sw}\left[-\frac{R_s}{L_l}\tilde{\imath}_{sw} - K_{zw}.sat(\tilde{\imath}_{sw})\right] \\ & + \tilde{\Omega}\left[\frac{5}{2}\frac{p\psi_f}{J_m}\left[\left(i_{s\beta}\cos\theta - i_{s\alpha}\sin\theta\right) - \left(\hat{\imath}_{s\beta}\cos\hat{\theta} - \hat{\imath}_{s\alpha}\sin\hat{\theta}\right)\right] - \frac{B_m}{J_m}\tilde{\Omega} - K_{\Omega}.sat(\tilde{\imath}_{s\alpha}) - K_{\Omega}.sat(\tilde{\imath}_{s\beta})\right] \\ & + \tilde{\theta}\left[\Omega - \hat{\Omega} - K_{\theta}.sat(\tilde{\imath}_{s\alpha}) - K_{\theta}.sat(\tilde{\imath}_{s\beta})\right] \end{aligned} \tag{32}$$

To simplify the design of the observer, equation (32) can be written as follows

$$\begin{aligned}\dot{V} = &-a_1\tilde{\imath}_{s\alpha}^2 + a_2\tilde{\imath}_{s\alpha}\left(\Omega\sin\theta - \hat{\Omega}\sin\hat{\theta}\right) - K_{\alpha\beta}|\tilde{\imath}_{s\alpha}| \\ &- a_3\tilde{\imath}_{s\beta}^2 + a_4\tilde{\imath}_{s\beta}\left(\hat{\Omega}\cos\hat{\theta} - \Omega\cos\theta\right) \\ &- K_{\alpha\beta}|\tilde{\imath}_{s\beta}| - a_6\tilde{\Omega}^2 \\ &+ a_5\tilde{\Omega}\left[\left(i_{s\beta}\cos\theta - i_{s\alpha}\sin\theta\right)\right. \\ &\left.- \left(\hat{\imath}_{s\beta}\cos\hat{\theta} - \hat{\imath}_{s\alpha}\sin\hat{\theta}\right)\right] \\ &- \tilde{\Omega}K_{\Omega}.sat(\tilde{\imath}_{s\alpha}) - \tilde{\Omega}K_{\Omega}.sat\left(\tilde{\imath}_{s\beta}\right) \\ &- a_7\tilde{\imath}_{sz}^2 - K_{zw}|\tilde{\imath}_{sz}| - a_7\tilde{\imath}_{sw}^2 - K_{zw}|\tilde{\imath}_{sw}| \\ &+ \tilde{\theta}\tilde{\Omega} - \tilde{\theta}K_{\theta}.sat(\tilde{\imath}_{s\alpha}) - \tilde{\theta}K_{\theta}.sat\left(\tilde{\imath}_{s\beta}\right)\end{aligned} \tag{33}$$

where $a_1 = \frac{R_s}{L_{s\alpha}}$, $a_2 = \frac{R_s}{L_{s\beta}}$, $a_3 = p\frac{\psi_f}{L_{s\alpha}}$, $a_4 = p\frac{\psi_f}{L_{s\beta}}$, $a_5 = \frac{5}{2}\frac{p\psi_f}{J_m}$, $a_6 = \frac{B_m}{J_m}$, $a_7 = \frac{R_s}{L_l}$.

The variables of the motor are defined by their nominal values such as nominal current, nominal speed, etc... It is satisfactory to consider that the observer initial conditions are specified with values less than the nominal ones. Thus, all terms of equation (33) can be bounded at time t=0 as follows:

$$\left|\Omega\sin\theta - \hat{\Omega}\sin\hat{\theta}\right| < 2\Omega_{max}$$

$$\left|\bar{\imath}_{s\alpha}\left(\Omega\sin\theta - \hat{\Omega}\sin\hat{\theta}\right)\right| < 4i_{max}\Omega_{max}$$

Where

$$|\bar{\imath}_{s\alpha}| = \left|\bar{\imath}_{s\beta}\right| < 2i_{max}$$

And

$$\left|\bar{\imath}_{s\beta}\left(\hat{\Omega}\cos\hat{\theta} - \Omega\cos\theta\right)\right| < 4i_{max}\Omega_{max}$$

$$\left|\bar{\Omega}\left(sat(\bar{\imath}_{s\alpha}) + sat\left(\bar{\imath}_{s\beta}\right)\right)\right| < 4\Omega_{max}$$

$$\begin{aligned}\bar{\Omega}\left[\left(i_{s\beta}\cos\theta - i_{s\alpha}\sin\theta\right) - \left(\hat{\imath}_{s\beta}\cos\hat{\theta} - \hat{\imath}_{s\alpha}\sin\hat{\theta}\right)\right] \\ < 8i_{max}\Omega_{max}\end{aligned}$$

$$\left|\bar{\theta}\bar{\Omega}\right| < 4\theta_{max}\Omega_{max}$$

$$|\bar{\imath}_{sz}| = |\bar{\imath}_{sw}| < 2i_{max}$$

In order to satisfy those conditions at t = 0: thus, it is achievable by choosing the gains of the observer in order to allow at $t > 0$ the convergence of the observer. Knowing that $-a_1\bar{\imath}_{s\alpha}^2 < 0$, $-a_3\bar{\imath}_{s\beta}^2 < 0$, $-a_6\bar{\Omega}^2 < 0$, $-a_7\bar{\imath}_{sz}^2 < 0$, $-a_7\bar{\imath}_{sw}^2 < 0$.

In order to assure the convergence of the observer presented in equation (30), it is satisfactory to choose the gains as $K_{\alpha\beta} > a_4\Omega_{max}$, $K_{\Omega} > 2a_5 i_{max}$, $K_{\theta} > \Omega_{max}$ and $K_{zw} > 0$.

V. DESIGN OF MRAS FOR FIVE PHASE PMSM

In order to observe the position and the rotor speed, a Model reference adaptive system (MRAS) is developed. The objective to design this observer for the FPMSM is to reduce the torque and speed fluctuations corresponding to a load change. Nonetheless, the MRAS strategy form the use of two separate motor models of various arrangement in order to observe the same state variable such as rotor flux, back EMF, current, reactive power articulated on various sets of an input variables. The dynamic error z of the observed and actual output is used to the adaptation structure which outputs the observer speed $\hat{\omega}$. This observed speed is followed by the integrator to obtain the estimated position $\hat{\theta}$. After that, this observed speed is utilized to determinate the adjustable model until the convergence of the error z to zero and that makes the observed speed and actual speed ω equal.

Consequently, two different models are used in the MRAS: the first is the reference model, it is utilized for identifying the two components of the stator currents along (in the Park reference frame) from the direct measurement of the currents in the stator reference frame. Meanwhile, the second is the adjustable model; it is used for the estimation of two components of the stator currents from direct measurement of stator currents and voltages. By eliminating the difference between the stator currents of the reference and adjustable models, one can estimate the rotor speed.

An adaptation mechanism, generally a PI controller is sufficient to make the behavior of the adaptive model tends towards the behavior of the reference model. The structure of the rotor speed estimation by the MRAS method is represented in Fig. 6.

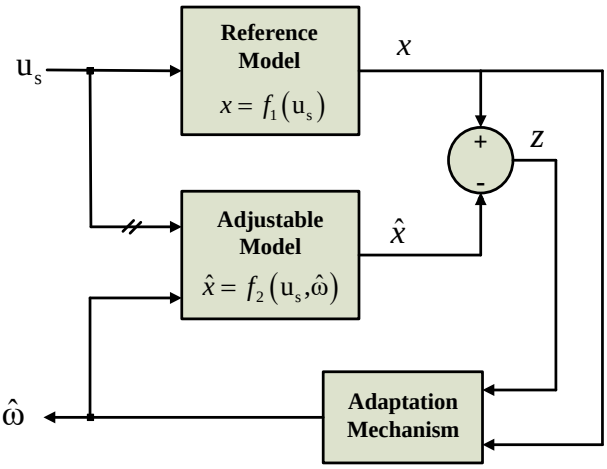

Fig. 6. Configuration of MRAS observer for five-phase PMSM

To estimate the rotor speed by the MRAS technique, it is necessary to choose a reference frame linked to the rotor. This transformation uses the position of the rotor which is estimated by the adaptive method of the reference model. To have a sensor less control in a reference frame linked to the stator, it is essential to use the Clark transformation which uses the axis marks (d, q, x, y) provided that you know the initial position of the rotor perfectly. By presenting the dynamic model of the five-phase PMSM, in a frame aligned with the rotor (d, q, x, y), one can develop two stator current estimators in this frame, using the measurements of stator currents and voltages.

After transformation and arrangement of the equations by making the necessary manipulations and transformations,

we arrive at the state model of the FPMSM expressed in the reference (d, q, x, y):

$$\begin{cases} \dot{x} = Ax + Bu + C \\ y = Ix \end{cases} \tag{34}$$

where $x = [i_{sd} \quad i_{sq} \quad i_{sx} \quad i_{sy}]^T$, $u = [u_{sd} \quad u_{sq} \quad u_{sx} \quad u_{sy}]^T$, $y = [i_{sd} \quad i_{sq} \quad i_{sx} \quad i_{sy}]^T$

$$A = \begin{pmatrix} \frac{-R_s}{L_d} & \frac{\omega L_q}{L_d} & 0 & 0 \\ \frac{-\omega L_d}{L_q} & \frac{-R_s}{L_q} & 0 & 0 \\ 0 & 0 & \frac{-R_s}{L_l} & 0 \\ 0 & 0 & 0 & \frac{-R_s}{L_l} \end{pmatrix},$$

$$B = \begin{pmatrix} \frac{1}{L_d} & 0 & 0 & 0 \\ 0 & \frac{1}{L_q} & 0 & 0 \\ 0 & 0 & \frac{1}{L_l} & 0 \\ 0 & 0 & 0 & \frac{1}{L_l} \end{pmatrix}, C = \begin{pmatrix} 0 \\ -\frac{\psi_f \omega}{L_q} \\ 0 \\ 0 \end{pmatrix},$$

$$I = \begin{pmatrix} 1 & 0 & 0 & 0 \\ 0 & 1 & 0 & 0 \\ 0 & 0 & 1 & 0 \\ 0 & 0 & 0 & 1 \end{pmatrix}.$$

Knowing that the two models (reference and adjustable) use the same inputs (stator voltages), one then defines the deviations of the stator currents as

$$\begin{cases} z_d = i_{sd} - \hat{\imath}_{sd} \\ z_q = i_{sq} - \hat{\imath}_{sq} \\ z_x = i_{sx} - \hat{\imath}_{sx} \\ z_y = i_{sy} - \hat{\imath}_{sy} \end{cases} \tag{35}$$

The derivatives of (35) can be then expressed by

$$\begin{cases} \frac{dz_d}{dt} = \frac{-R_s}{L_d} z_d + \frac{L_q}{L_d} \omega i_{sq} - \frac{L_q}{L_d} \hat{\omega} \hat{\imath}_{sq} \\ \frac{dz_q}{dt} = \frac{-R_s}{L_q} z_q - \frac{L_d}{L_q} \omega i_{sd} + \frac{L_d}{L_q} \hat{\omega} \hat{\imath}_{sd} + \frac{\psi_f}{L_q} \hat{\omega} - \frac{\psi_f}{L_q} \omega \\ \frac{dz_x}{dt} = \frac{-R_s}{L_l} z_x \\ \frac{dz_y}{dt} = \frac{-R_s}{L_l} z_y \end{cases} \tag{36}$$

By adding and subtracting the terms $\frac{L_q}{L_d} \hat{\omega} \hat{\imath}_{sq}$ and $\frac{L_d}{L_q} \hat{\omega} \hat{\imath}_{sd}$ to the first and second equalities in (36), it can be rewritten as

$$\begin{cases} \frac{dz_d}{dt} = \frac{-R_s}{L_d} z_d + \frac{L_q}{L_d} \hat{\omega} z_q + \frac{L_q}{L_d} (\omega - \hat{\omega}) i_{sq} \\ \frac{dz_q}{dt} = \frac{-R_s}{L_q} z_q - \frac{L_d}{L_q} \hat{\omega} z_d - \frac{L_d}{L_q} (\omega - \hat{\omega}) i_{sd} - \frac{\psi_f}{L_q} (\omega - \hat{\omega}) \\ \frac{dz_x}{dt} = \frac{-R_s}{L_l} z_x \\ \frac{dz_y}{dt} = \frac{-R_s}{L_l} z_y \end{cases} \tag{37}$$

Equation (37) can be expressed in a matrix form by

$$\begin{pmatrix} \frac{dz_d}{dt} \\ \frac{dz_q}{dt} \\ \frac{dz_x}{dt} \\ \frac{dz_y}{dt} \end{pmatrix} = \begin{pmatrix} \frac{-R_s}{L_d} & \frac{\hat{\omega} L_q}{L_d} & 0 & 0 \\ \frac{-\hat{\omega} L_d}{L_q} & \frac{-R_s}{L_q} & 0 & 0 \\ 0 & 0 & \frac{-R_s}{L_l} & 0 \\ 0 & 0 & 0 & \frac{-R_s}{L_l} \end{pmatrix} \begin{pmatrix} z_d \\ z_q \\ z_x \\ z_y \end{pmatrix} + \begin{pmatrix} \frac{L_q}{L_d} i_{sq} \\ -\frac{L_d}{L_q} i_{sd} - \frac{\psi_f}{L_q} \\ 0 \\ 0 \end{pmatrix} (\omega - \hat{\omega}) \tag{38}$$

Finally, one can write the estimation error in the state equation form as follows:

$$\frac{d}{dt}[z] = A[z] + [W] \tag{39}$$

Where $[z]$ is the error between the adjustable and reference models, $[W]$ is the feedback block, which constitutes the input of the linear block. Equations (38) and (39) constitute a nonlinear feedback system represented by Fig. 7. Indeed, this system can be schematized by a linear block described by the transfer matrix $H(s) = (s[I] - [A])^{-1}$ and a non-linear part of input $z(t)$ and output $W(z, t)$.

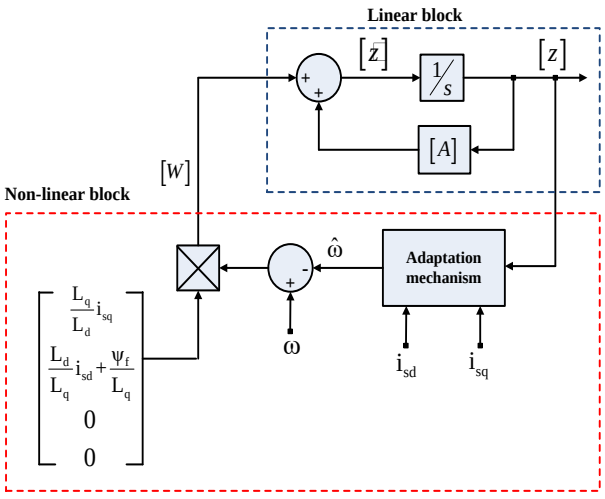

Fig. 7. MRAS adaptation system for five phase PMSM

The mandatory and adequate condition for the feedback system to be hyperstable is that $H(s)$ is a rigidly positive real matrix or by equivalence that all the poles of the elements of this matrix are with negative real parts. The study of the poles diagram of the transfer matrix $H(s)$, relative to the FPMSM, is given by Fig. 9. From the locations of the poles, we can notice that the real parts of the poles of $H(s)$ are negative. Finally, one can conclude that the matrix $H(s)$ is a positive definite matrix. After having shown that the transfer matrix $H(s)$ is defined positive, one will present in the next section the stability study of the MRAS observer.

VI. Stability Study Of the MRAS Observer

To manage the stability issue in this system, the Popov's hyper stability theory is used. To be considered hyper stable, the feedback block must fulfill the Popov's inequality:

$$\int_0^t [z]^T [W] dt \geq -\rho^2 \quad \text{for } t \geq 0 \tag{40}$$

where ρ is a time independent positive constant. The estimate of the speed is expressed by

$$\hat{\omega} = \xi_1 [z] + \xi_2 \int_0^t [z]\, dt \tag{41}$$

where ξ_1 and ξ_2 are non-linear functions of z_d and z_q.

Utilizing the definition of $[W]$, the relation (40) tends to be

$$\int_0^t \left(\left(z_d \frac{L_q}{L_d} i_{sq} \right) - z_q \left(\frac{L_d}{L_q} i_{sd} + \frac{\psi_f}{L_q} \right) \right) (\omega - \hat{\omega}) dt \geq -\rho^2 \tag{42}$$

Using (41), Popov's criterion for the actual system becomes:

$$\int_0^t \left(\left(z_d \frac{L_q}{L_d} i_{sq} \right) - z_q \left(\frac{L_d}{L_q} i_{sd} + \frac{\psi_f}{L_q} \right) \right) \left(\omega - \xi_1 [z] - \xi_2 \int_0^t [z]\, dt \right) dt \geq -\rho^2 \tag{43}$$

A solution of this inequality can be obtained using the following relationship [63, 64],

$$\int_0^t k \left[\frac{d}{dt} f(t) \right] f(t) dt = \frac{1}{2} k [f^2(t) - f^2(0)] \geq -\frac{1}{2} k f^2(0), k > 0 \tag{44}$$

Then, from (43) and (44), the expressions of ξ_1 and ξ_2 can be expressed as follows:

$$\begin{aligned} \xi_1 &= K_1 \left(\frac{L_q}{L_d} i_{sq} z_d - \frac{L_d}{L_q} i_{sd} z_q - \frac{\psi_f}{L_q} z_q \right) \\ \xi_2 &= K_2 \left(\frac{L_q}{L_d} i_{sq} z_d - \frac{L_d}{L_q} i_{sd} z_q - \frac{\psi_f}{L_q} z_q \right) \end{aligned} \tag{45}$$

Where K_1 and K_2 are the adaptation gains and they are positive constants.

It is worth mentioning that the nonlinear functions ξ_1 and ξ_2 obtained in (45), can be also obtained using Lyapunov stability check theory for different types of machines as presented in [65], in which the nonlinear functions are derived in terms of the current errors and estimated stator or rotor flux components.

From the general structure of the adaptation mechanism, the estimation of the rotation speed $\hat{\omega}$ is a function of the error z. In order to enhance the dynamic of the adaptation regime, a PI regulator is used in order to estimate the speed. Thus the speed estimation can be expressed using the following formula,

$$\begin{aligned} \hat{\omega} = K_p &\left(\frac{L_q}{L_d} i_{sq} z_d - \frac{L_d}{L_q} i_{sd} z_q - \frac{\psi_f}{L_q} z_q \right) \\ &+ K_i \int_0^t \left(\frac{L_q}{L_d} i_{sq} z_d - \frac{L_d}{L_q} i_{sd} z_q - \frac{\psi_f}{L_q} z_q \right) dt \end{aligned} \tag{46}$$

Where K_p and K_i are the PI constants to correct the error between the actual and observed speeds. At last, the observed rotor position is acquired by integrating the estimated speed by

$$\hat{\theta} = \int_0^t \hat{\omega} dt + \theta(0) \tag{47}$$

Where $\theta(0)$ represents the initial position. Thus, the proper adaptation mechanism is obtained using Popov's hyper stability criterion [64, 66, 67]. This integral law guarantees the stability of the global system. In this phase, we consider that the two parameters $\hat{\omega}$ and ω vary at course of time, and each can be considered as an input to (34). The study of the dynamic response of the rotor speed estimation requires a linearization of the error equations for a small variation around an operating point. Consequently, the variations of the error are described by the following equation:

$$\Delta z(t) = z(t) - z(t - \Delta t) \tag{48}$$

To get better performance, the flux oriented control principle is adopted. This type of control aims to canceling the stator current along the direct axis. Actually, this property will then be used in the calculation of the transfer function which links Δz_ω with $\Delta\hat{\omega}$. Then, by substituting from (45) into (39), the transfer function which links Δz_ω with $\Delta\hat{\omega}$ is obtained as follows

$$\left. \frac{\Delta z_\omega}{\Delta \hat{\omega}} \right|_{\Delta\omega=0} = G(s) = \frac{K_L^2 (s + T_d) + K_L i_{sq} \omega}{(s + T_d)(s + T_q) + \omega^2} \tag{49}$$

where $T_d = \frac{R_s}{L_d}$, $T_q = \frac{R_s}{L_q}$ and $K_L = \frac{\psi_f}{L_q}$.

The closed loop block diagram of the dynamic response of the estimation of the rotor speed by the MRAS method is given by Fig. 8.

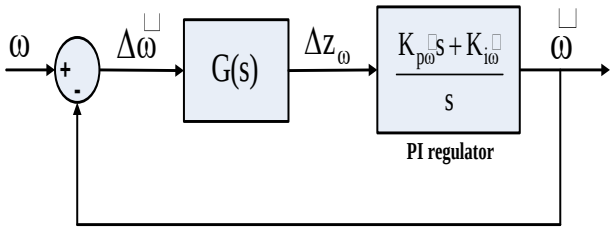

Fig. 8. Closed-loop block diagram of MRAS based speed estimation

From Fig. 8, the transfer function that relates $\Delta\hat{\omega}$ with ω is expressed by:

$$\frac{\hat{\omega}}{\Delta\hat{\omega}} = G(s) * \frac{K_{p\hat{\omega}}s + K_{i\hat{\omega}}}{s} \quad (50)$$

The choice of the values of $K_{p\hat{\omega}}$ and $K_{i\hat{\omega}}$ was determined in order to obtain an overall stability of the system. This choice is validated via studying the placement of the observer poles and the poles of the system. The range of variation of ω which fulfills this condition, determined by analyzing the locus of the poles of the system, is $\omega = [-320,320]$. In this interval, with a step of 1 rad/s, all the closed-loop poles are at negative real parts and therefore, the system is stable over the entire range of variation of ω. The placement of poles of the closed loop system in the complex plane with $K_{p\hat{\omega}} = 150$ and $K_{i\hat{\omega}} = 4000$ is shown in Fig. 9.

The placement of the poles in the complex plane made it possible to show that the gains for the speed estimator are adequate in order to avoid instability problems.

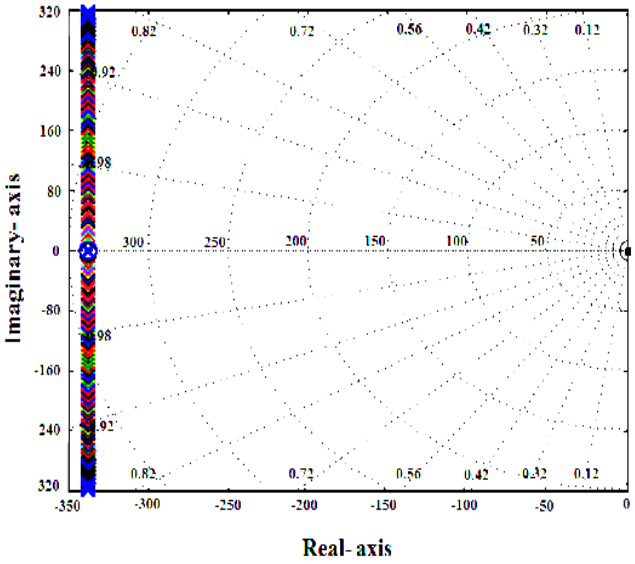

Fig. 9. Closed-loop system pole placement for the MRAS observer

After designing the SMO and MRAS observers, the overall vector control scheme is drawn as shown in Fig. 10. The measured currents and voltages are utilized as input to either of the SMO observer or MRAS observer, from which the estimated rotor speed $\hat{\omega}$ and rotor position $\hat{\theta}$ are obtained. The estimated speed is then used to close the speed control loop, meanwhile the estimated position is used for co-ordinates transformation. The *d*, *q*, *x*, *y* stator current components are compared with their relevant references and the errors are fed to the designed PI current controllers to generate the reference voltages u^*_{sdqxy} which are then transformed to $u^*_{s\alpha\beta zw}$ voltages to be fed to the PWM algorithm to generate the switching states of the five-phase inverter. It is worth mentioning that both estimators are shown in the overall schematic but each of them is used separately.

VII. Drive Performance without Parameters Variation

A. With SMO observer

In this test the five-phase PMSM drive is tested using the designed SMO without subjecting the system to any uncertainties like parameters variation. The drive is subjected to a speed change profile of $0 \rightarrow 850 \rightarrow -850$ at time of $0 \rightarrow 0.05 \rightarrow -0.45$ s, respectively. A 4 Nm load torque is applied at time t=0.25 s. From the illustrated figures, the designed vector control and SMO observer are clearly demonstrating their effectiveness.

Fig. 11 shows that the estimated speed using the designed SMO tracks precisely the actual speed, with minimum deviation. The speed estimation error is also presented in Fig. 12, which approve the validity of the SMO. Figs. 13 and 14 also confirm the validness of the SMO through the definite observation of rotor position, and the minimum mismatch, respectively.

Fig. 15 presents the developed motor torque and which validate the affectivity of the designed vector control system through tracking definitely the reference torque. Figs. 16 and 17 are also reconfirming the validity of the designed controller, as the *d*-axis current is kept at zero, meanwhile the *q*-axis current follow the variation of the torque.

Figs. 18, 19, 20 and 21 show respectively, the actual and estimated values of α, β, *z*, *w* stator currents, and their related estimation errors. From these illustrations, it is confirmed that the designed SMO succeeded in achieving high estimation precision for the currents. Finally, Fig. 22 illustrates the five-phase stator currents.

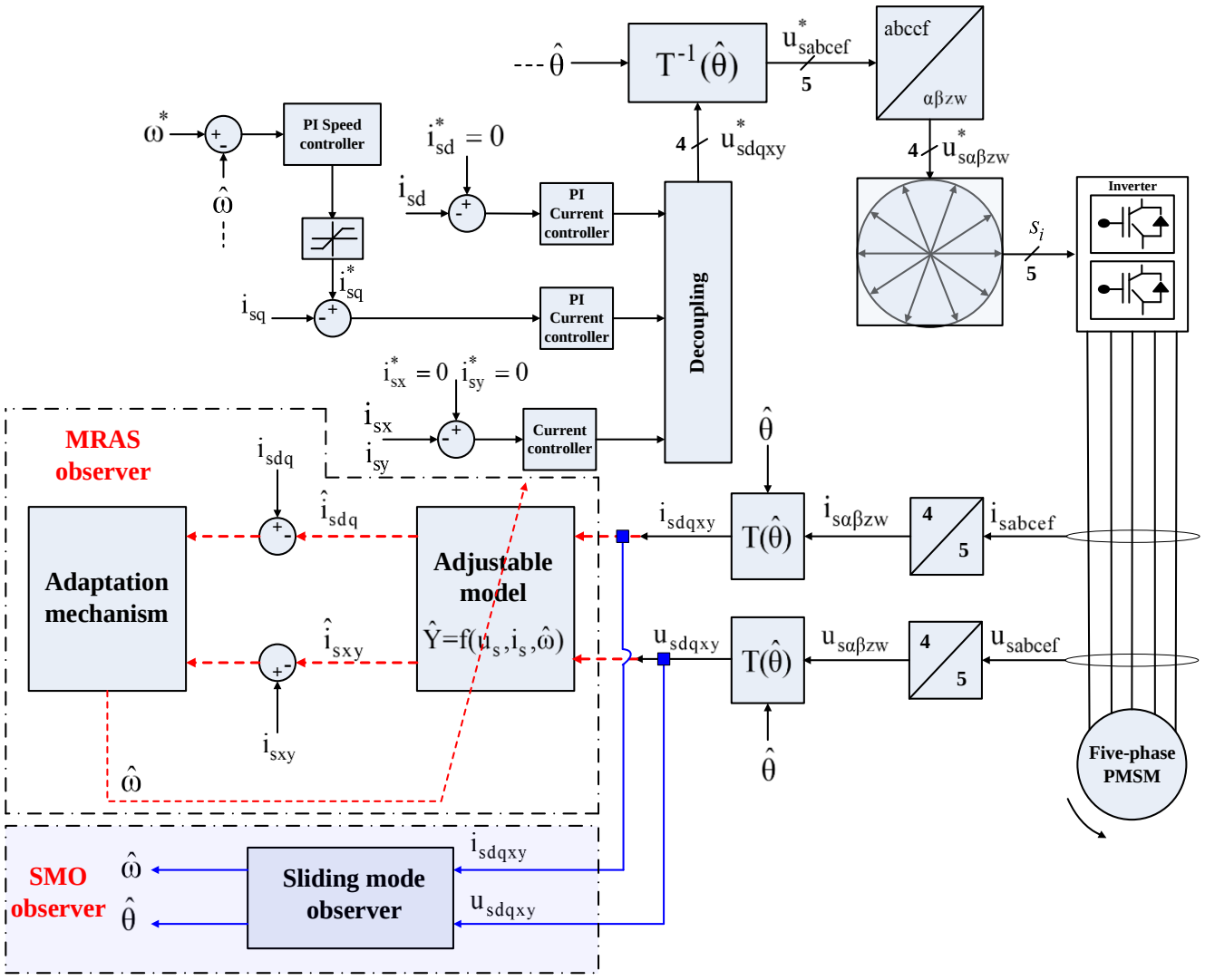

Fig. 10. Schematic diagram of the sensorless vector controlled five-phase PMSM

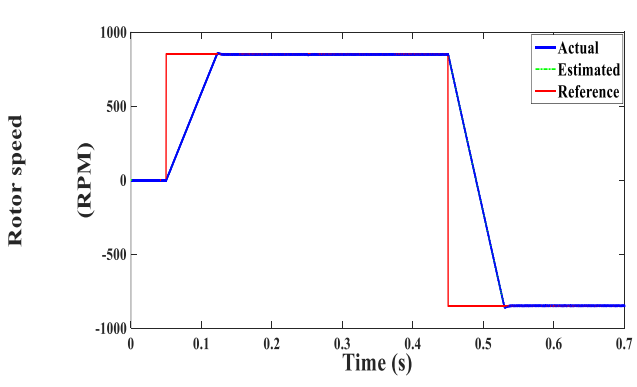

Fig. 11. Rotor speed with SMO observer

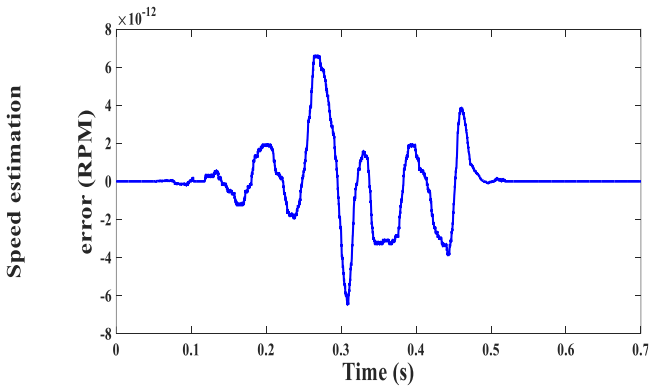

Fig. 12. Speed estimation error with SMO

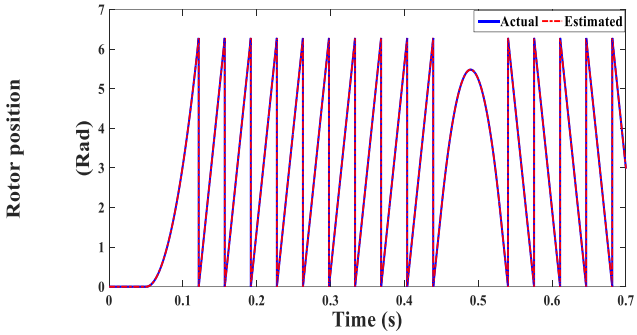

Fig. 13. Rotor position using SMO

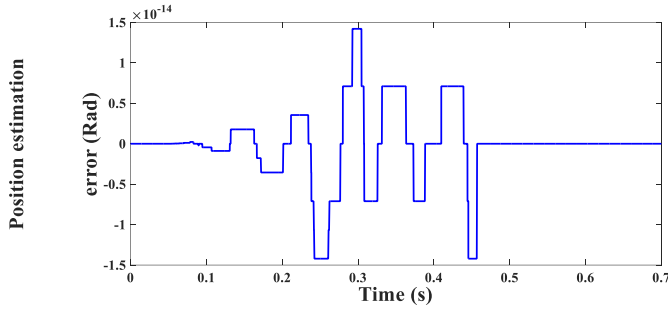

Fig. 14. Rotor position estimation error using SMO

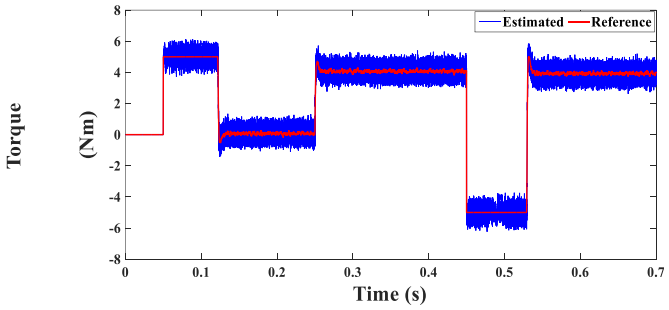

Fig. 15. Developed torque with SMO

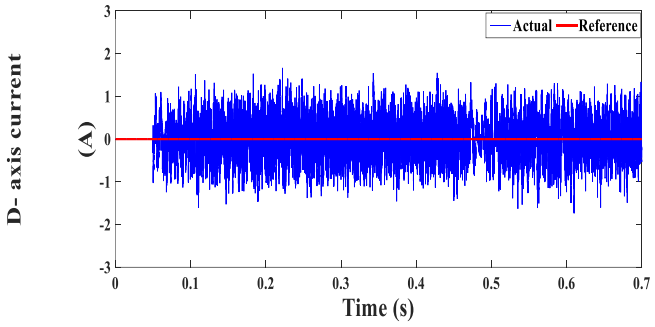

Fig. 16. D-axis current component

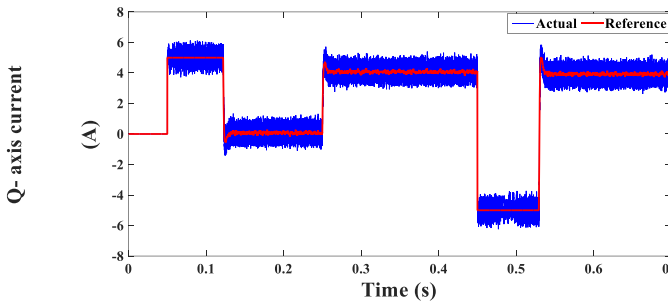

Fig. 17. Q-axis current component

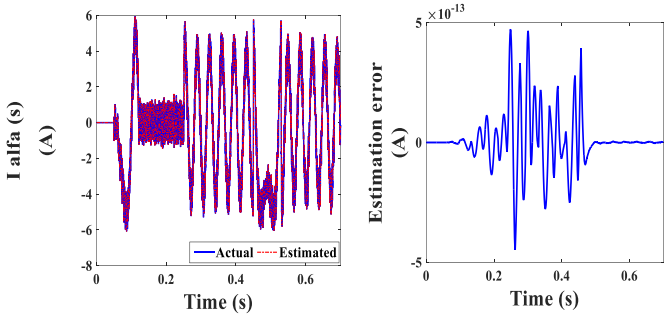

Fig. 18. α-axis current component and relevant estimation error

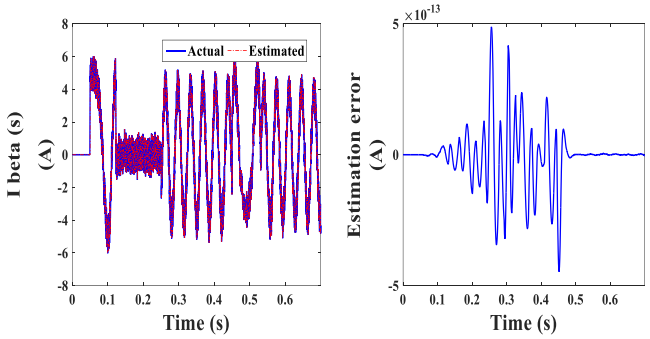

Fig. 19. β-axis current component and relevant estimation error

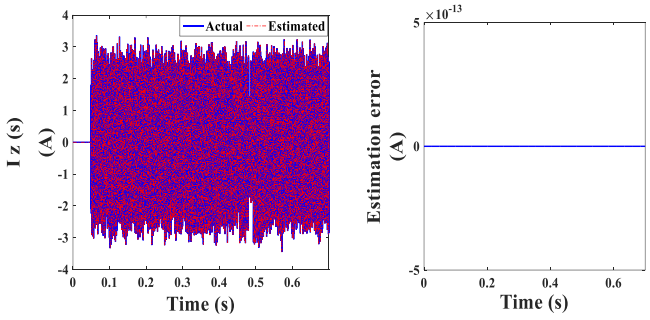

Fig. 20. Z-axis current component and relevant estimation error

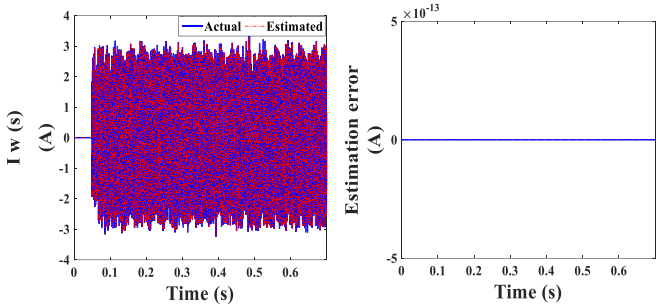

Fig. 21. w-axis current component and relevant estimation error

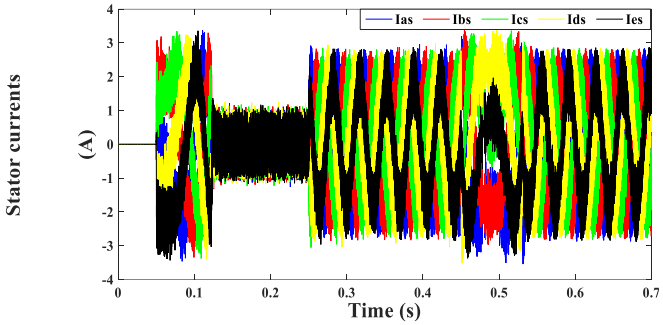

Fig. 22. Stator currents when considering SMO observer

B. With MRAS observer

The same test conditions accomplished with the SMO are also adopted with the MRAS observer. This is to visualize the differences between the two estimators. Figs. 23 and 24 show the estimated and actual speeds and the resulted estimation error. Comparing Fig. 24 with Fig. 12, it is revealed that however the MRAS observer presents sufficient performance in speed estimation, but the estimation error under MRAS is much higher than that of SMO. The same remark is noticed from Figs. 25 and 26, which represent the estimated and actual rotor position and its estimation error. The high performance of the vector control is also approved with the MRAS through the appropriate tracking of reference torque as in Fig. 27 and direct and quadrature reference currents as in Figs. 28 and 29, respectively. Figs. 30, 31, 32 show the actual and estimated stator current components α, β, z, w and their related estimation errors. These figures reveal that the MRAS presents an appropriate estimation process for normal operation (without considering uncertainties in the system). At last, the five-phase stator currents are shown in Fig. 33.

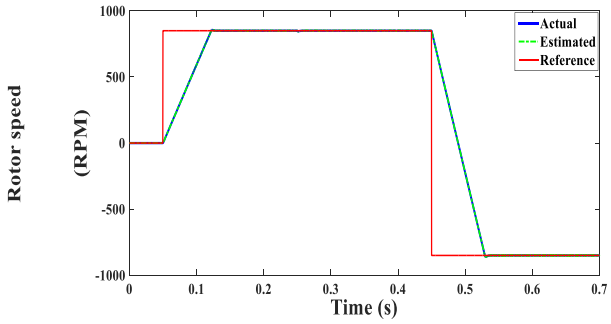

Fig. 23. Rotor speed with MRAS observer

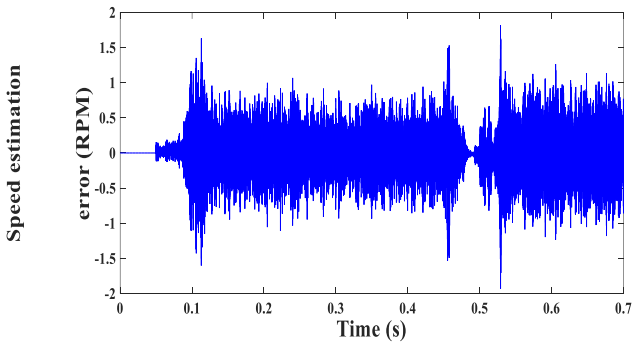

Fig. 24. Speed estimation error with MRAS observer

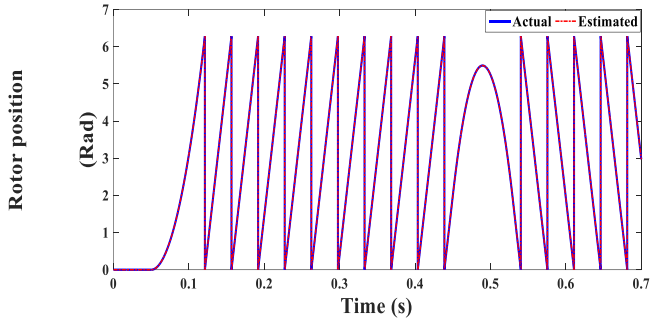

Fig. 25. Rotor position with MRAS observer

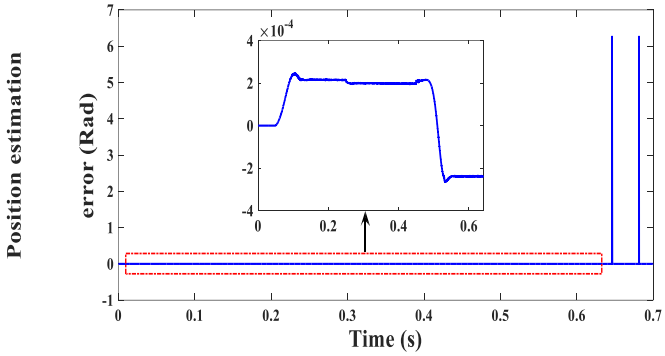

Fig. 26. Rotor position estimation error using MRAS

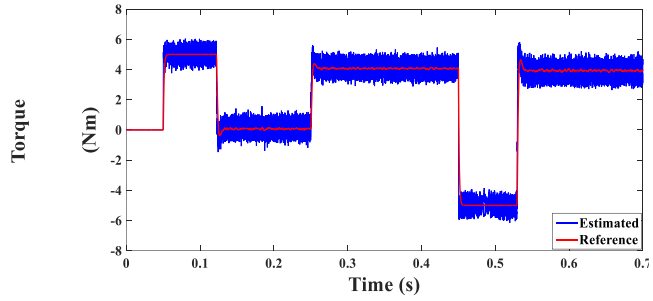

Fig. 27. Developed torque with MRAS

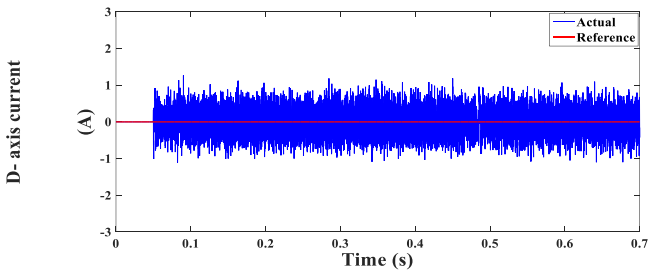

Fig. 28. D-axis current component

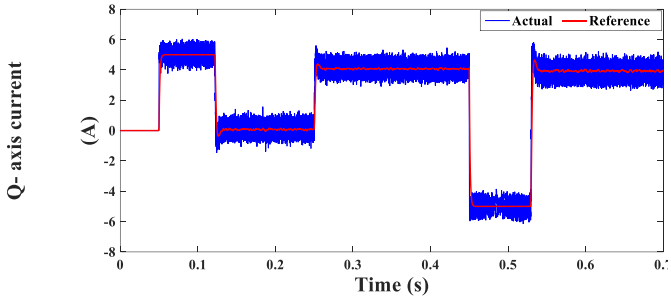

Fig. 29. Q-axis current component

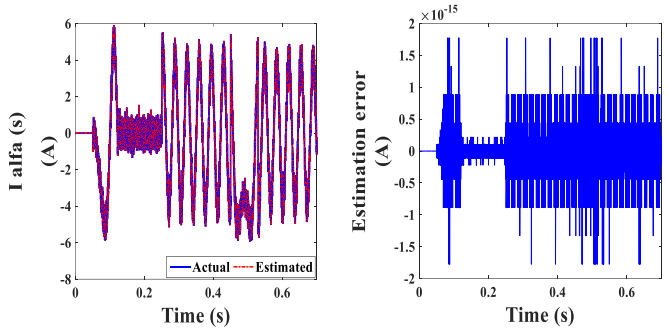

Fig. 30. α-axis current and estimation error with MRAS

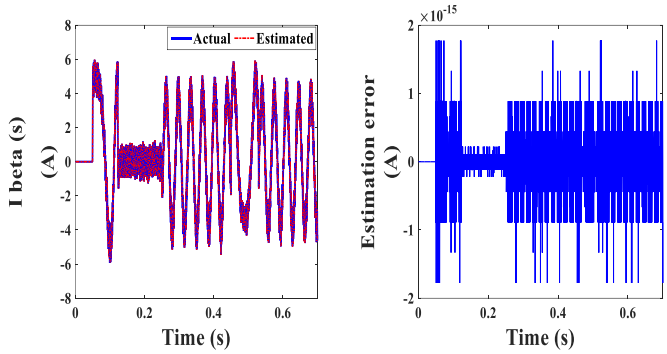

Fig. 31. β-axis current and estimation error with MRAS

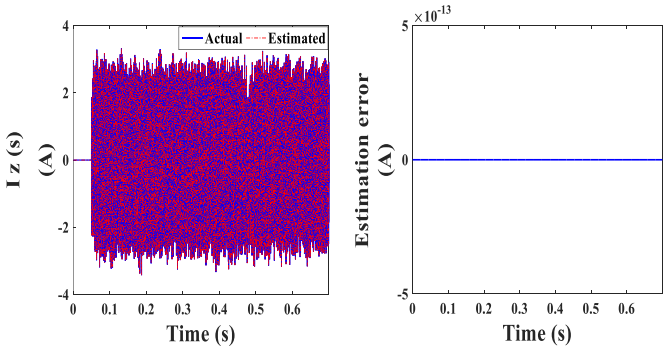

Fig. 32. Z-axis current and estimation error with MRAS

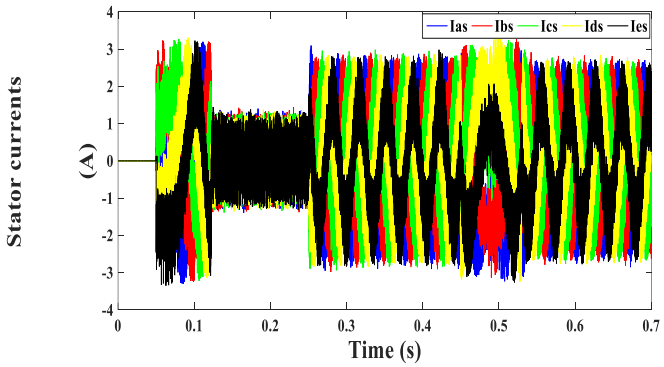

Fig. 33. Five-phase stator currents using MRAS observer

VIII. TESTING BOTH ESTIMATORS UNDER STATOR RESISTANCE VARIATION

In this test, both estimators are tested when considering a mismatch in the stator resistance (R_s) of 1.10 times its original value. The mismatch is made at time t=0.35 s, as illustrated in Fig. 34. Furthermore, the speed is changed from 850 RPM to 10 RPM to testify the ability of the estimators in working at low frequencies. A load torque of 4 Nm is applied at time t=0.25 s. The effect of R_s variation on both SMO and MRAS performances are synthesized in Figs. 35 and 36, which show the estimated and actual speed values and their resultant deviation, respectively. It can be deduced that the SMO estimator has the superiority over the MRAS in maintaining the normal dynamic behavior even though there is a parameter mismatch. On the other hand, the performance of MRAS is rapidly degraded resulting in high estimation error. These remarks are also observed in Figs. 37 and 38, which outline the estimated and actual rotor positions and the corresponding estimation error, respectively. Another illustration, which clarifies the robustness of the SMO in comparison with the MRAS observer, can be shown via Fig. 39 that views the calculated values of motor torque. The SMO is successfully overcome the effect of R_s variation, meanwhile the MRAS failed in facing the variation.

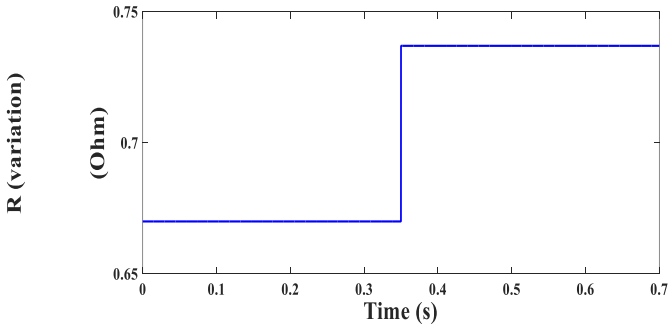

Fig. 34. Resistance variation

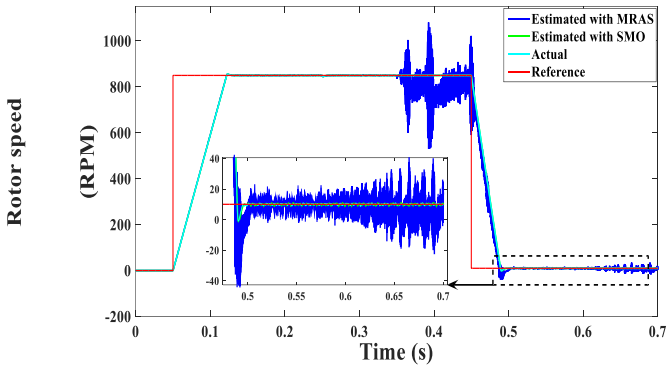

Fig. 35. Rotor speed under R mismatch

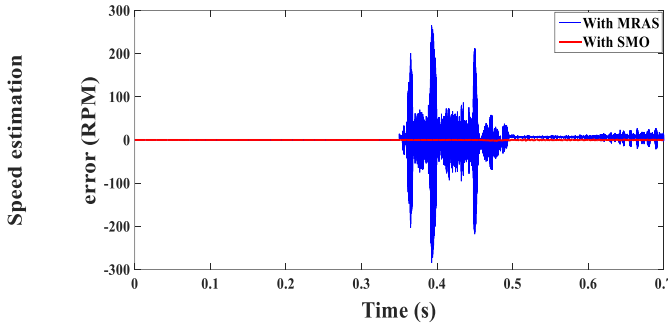

Fig. 36. Speed deviation under R mismatch

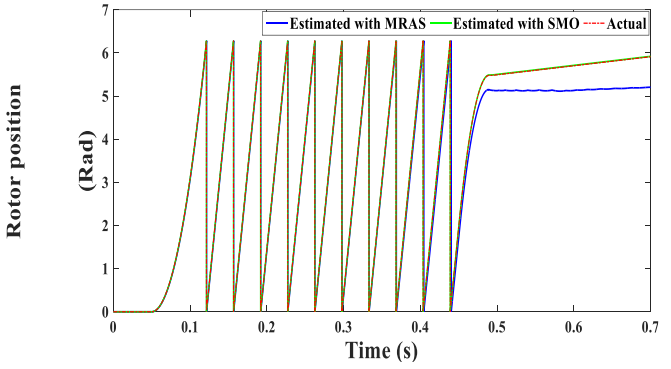

Fig. 37. Rotor position variation under R mismatch

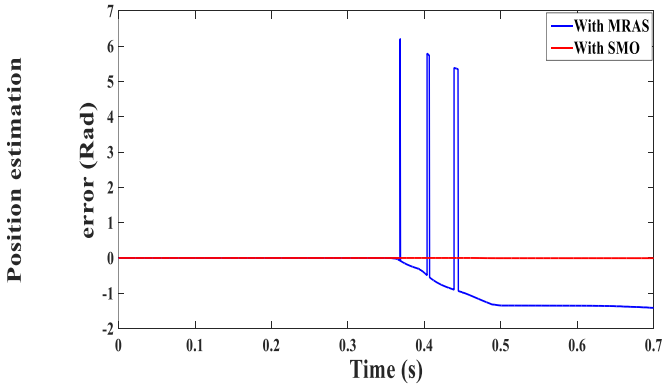

Fig. 38. Position estimation error under R mismatch

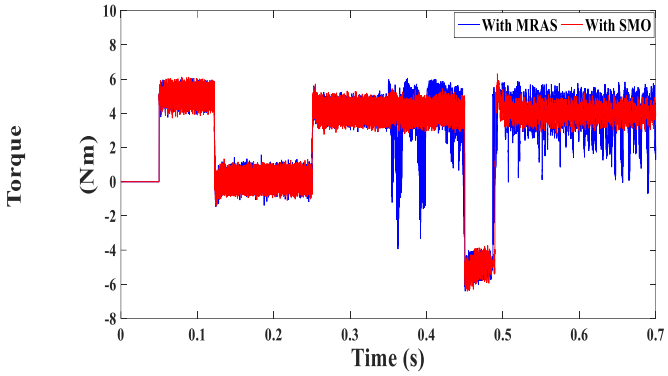

Fig. 39. Developed torque under R mismatch

IX. TESTING BOTH ESTIMATORS UNDER STATOR INDUCTANCE VARIATION

The performance of the two observers is also tested when considering a mismatch of 20% of the stator inductance value. The inductance variation is applied at time t=0.35 s as shown in Fig. 40. The speed is varied from 850 RPM to 10 RPM to verify the estimators' capability in covering all speed ranges. A 4 Nm load torque is considered at time t=0.25 s. The inductance variation impact on both observers is noticed in Figs. 41 and 42, which illustrate the observed and real speed values and their relative deviation, respectively. It can be confirmed that the SMO observer demonstrates better dynamics compared with the MRAS. Alternatively, the MRAS performance is quickly deteriorated, which results in high speed estimation error. These remarks are also observed in Figs. 43 and 44, which show the real and observed rotor positions and the resultant error, respectively. The robustness of the SMO can be also confirmed by checking the torque profile in Fig. 45. The SMO is successfully overcome the inductance variation effect; alternatively, the MRAS failed in maintaining a robust operation for the drive.

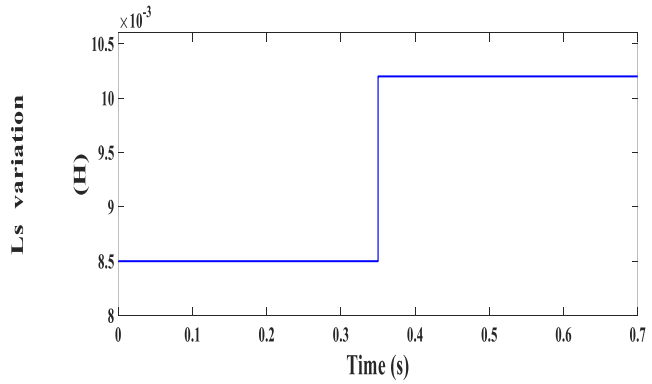

Fig. 40. Inductance variation

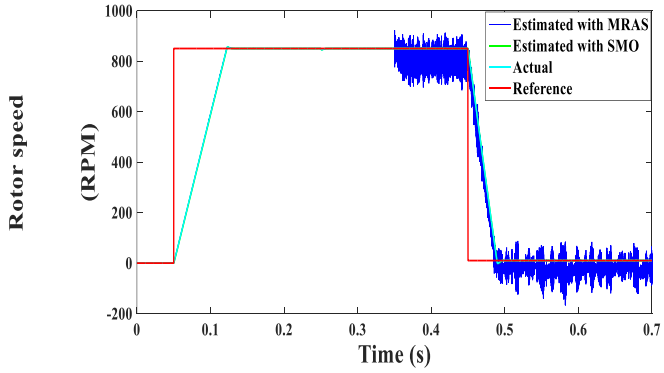

Fig. 41. Rotor speed under Ls mismatch

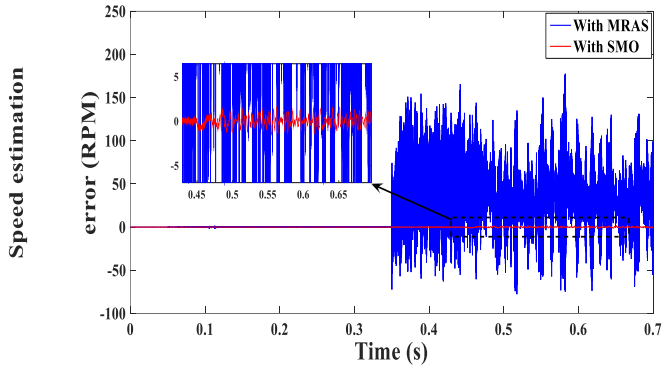

Fig. 42. Speed deviation under Ls mismatch

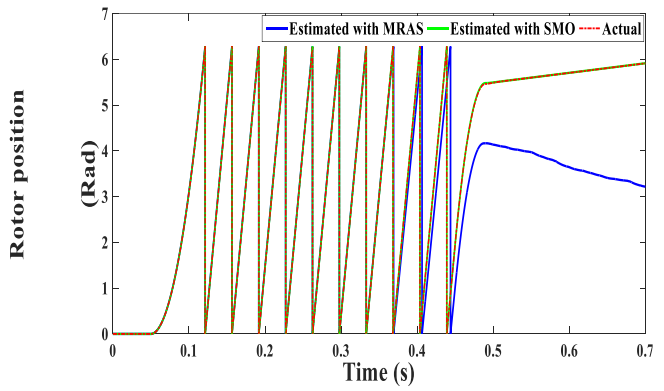

Fig. 43. Rotor position variation under Ls mismatch

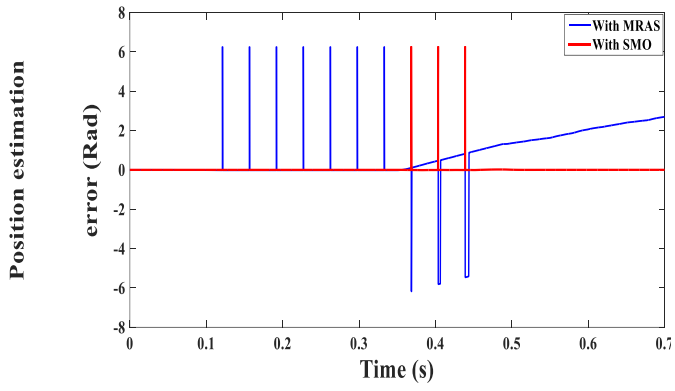

Fig. 44. Position estimation error under Ls mismatch

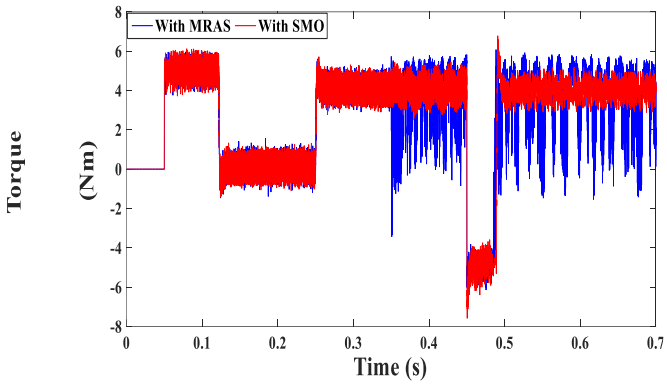

Fig. 45. Developed torque under Ls mismatch

X. CONCLUSION

The paper introduced a comprehensive performance analysis for a five-phase PMSM drive using two different sensorless schemes: SMO and MRAS observers. In addition to that, the drive itself is controlled using a vector control scheme which is designed in a systematic manner. The modeling of five-phase PMSM, SMO and MRAS observers are described in details to clarify the base operation of each observer. A stability check procedure is performed for both SMO and MRAS observers. Both estimators are tested with the vector control with and without considering parameters variation. It is found that under normal operation, both estimators are exhibiting an appropriate estimation for the speed, rotor position and stator currents as well giving the SMO a higher precision rate. However, under uncertainties (R_s and L_s are taken as cases of study), the performance of MRAS degraded obviously in comparison with the SMO which introduced high robustness against the variation. The degradation in the MRAS performance is observed through large estimation error and high speed and torque oscillations. Thus, it can be deduced that the designed SMO has succeeded in approving its robustness against the system uncertainties without incorporating any parameter observation procedure. Finally, one can propose the studying of dynamic behaviors of other multiphase machines (i.e. seven phase and nine phase) using these two observers after considering the physical structure of each machine type.

APPENDIX

TABLE II. PARAMETERS OF FIVE-PHASE PMSM

Symbol	Value
R	0.67 Ω
L_d	0.0085 H
L_q	0.0085 H
L_l	0.00093 H
ψ_f	0.2 Vs
U_{dc}	400 V
J_m	0.004 kg.m^2
p	2
T_n	4 Nm

TABLE III. PARAMETERS OF SPEED AND CURRENT CONTROLLERS

Symbol	Value
$K_{P\Omega}$	3.0155
$K_{I\Omega}$	1170
K_{Pd}	4.69
K_{Id}	2245
K_{Pq}	6.03
K_{Iq}	3507
K_{Pxy}	6.03
K_{Ixy}	12067

TABLE IV. PARAMETERS OF SMO

Symbol	Value
K_{α}	50
K_{β}	50
K_{z}	0.0001
K_{w}	0.0001
K_{Ω}	30
K_{θ}	1E-6

TABLE V. PARAMETERS OF MRAS

Symbol	Value
K_P	150
K_I	4000

REFERENCES

[1] X. Wang *et al*., "Torque Ripple Reduction in Sectored Multi Three-Phase Machines Based on PWM Carrier Phase Shift," *IEEE Transactions on Industrial Electronics*, vol. 67, no. 6, pp. 4315-4325, 2020.

[2] M. A. Mossa, "Effective Predictive Flux Control for a Five Phase Induction Motor Drive with Inverter Output Filter," *International Review of Electrical Engineering (IREE)*, vol. 13, no. 5, pp. 373-384, 2018.

[3] S. Rubino, R. Bojoi, D. Cittanti and L. Zarri, "Decoupled and Modular Torque Control of Multi-Three-Phase Induction Motor Drives," *IEEE Transactions on Industry Applications*, vol. 56, no. 4, pp. 3831-3845, 2020.

[4] M. A. Mossa and H. Echeikh, "A novel fault tolerant control approach based on backstepping controller for a five-phase induction motor drive: Experimental investigation," *ISA Trans*. 112, 373–385.

[5] G. Jing and C. Zhou, "Control Strategy for a Five-Leg Inverter Supplying Dual Three-Phase PMSM," *IEEE Access*, vol. 8, pp. 174480-174488, 2020.

[6] M. A. Mossa, Vu Quynh, H. Echeikh, T. D. Do, "Deadbeat-Based Model Predictive Voltage Control for a Sensorless Five-Phase Induction Motor Drive," *Mathematical Problems in Engineering*, vol. 2020, p. 4164526, 2020.

[7] G. Li, J. Hu, Y. Li and J. Zhu, "An Improved Model Predictive Direct Torque Control Strategy for Reducing Harmonic Currents and Torque Ripples of Five-Phase Permanent Magnet Synchronous Motors," *IEEE Transactions on Industrial Electronics*, vol. 66, no. 8, pp. 5820-5829, 2019.

[8] M. A. Mossa, H. Echeikh, A. A. Z. Diab, H. H. Alhelou, P. Siano, "Comparative Study of Hysteresis Controller, Resonant Controller and Direct Torque Control of Five-Phase IM under Open-Phase Fault Operation," *Energies*, vol. 14, p. 1317, 2021.

[9] M. Mossa, and A. Z. Diab, "Effective Model Predictive Control Approach for a Faulty Induction Motor Drive," *International Review of Electrical Engineering* (IREE), vol. 14, no. 5, pp. 314-327, 2019.

[10] S. Wu, C. Tian, W. Zhao, J. Zhou and X. Zhang, "Design and Analysis of an Integrated Modular Motor Drive for More Electric Aircraft," *IEEE Transactions on Transportation Electrification*, vol. 6, no. 4, pp. 1412-1420, 2020.

[11] M. A. Mossa, H. Echeikh, A. Iqbal, T. Duc Do, A. S. Al-Sumaiti," A novel sensorless control for multiphase induction motor drives based on singularly perturbed sliding mode observer-experimental validation," *Appl Sci*, vol. 10, no. 8, p. 2776, 2020.

[12] M. H. Vafaie, B. M. Dehkordi, P. Moallem and A. Kiyoumarsi, "Improving the Steady-State and Transient-State Performances of PMSM Through an Advanced Deadbeat Direct Torque and Flux Control System," *IEEE Transactions on Power Electronics*, vol. 32, no. 4, pp. 2964-2975, 2017.

[13] M. A. Mossa, O. Gam, N. Bianchi and N. V. Quynh, "Enhanced Control and Power Management for a Renewable Energy-Based Water Pumping System," *IEEE Access*, vol. 10, pp. 36028-36056, 2022.

[14] A. V. Sant, K. R. Rajagopal and N. K. Sheth, "Permanent Magnet Synchronous Motor Drive Using Hybrid PI Speed Controller With Inherent and Noninherent Switching Functions," *IEEE Transactions on Magnetics*, vol. 47, no. 10, pp. 4088-4091, Oct. 2011.

[15] M. A. Mossa, H. Echeikh and N. V. Quynh, "A Novel Sensorless Predictive Voltage Control for an Induction Motor Drive Based on a Back-Stepping Observer-Experimental Validation," *IEEE Access*, vol. 9, pp. 11921-11942, 2021.

[16] M. A. Mossa, H. Echeikh, A. Iqbal, T. Duc Do, AS. Al-Sumaiti, "A novel sensorless control for multiphase induction motor drives based on singularly perturbed sliding mode observer-experimental validation," *Appl Sci*, vol. 10, p. 2776, 2020.

[17] X. Luo, Q. Tang, A. Shen and Q. Zhang, "PMSM Sensorless Control by Injecting HF Pulsating Carrier Signal Into Estimated Fixed-Frequency Rotating Reference Frame," *IEEE Transactions on Industrial Electronics*, vol. 63, no. 4, pp. 2294-2303, 2016.

[18] S. Wang, K. Yang and K. Chen, "An Improved Position-Sensorless Control Method at Low Speed for PMSM Based on High-Frequency Signal Injection into a Rotating Reference Frame," *IEEE Access*, vol. 7, pp. 86510-86521, 2019.

[19] J. M. Liu and Z. Q. Zhu, "Novel Sensorless Control Strategy With Injection of High-Frequency Pulsating Carrier Signal Into Stationary Reference Frame," *IEEE Transactions on Industry Applications*, vol. 50, no. 4, pp. 2574-2583, 2014.

[20] C. Choi and J. Seok, "Compensation of Zero-Current Clamping Effects in High-Frequency-Signal-Injection-Based Sensorless PM Motor Drives," *IEEE Transactions on Industry Applications*, vol. 43, no. 5, pp. 1258-1265, 2007.

[21] Z. Lin, X. Li, Z. Wang, T. Shi and C. Xia, "Minimization of Additional High-Frequency Torque Ripple for Square-Wave Voltage Injection IPMSM Sensorless Drives," *IEEE Transactions on Power Electronics*, vol. 35, no. 12, pp. 13345-13355, 2020.

[22] J. Liu and J. Chen, "A Changeover of Rotor Position Estimation between Rotor Speed Adaptive Stator Flux Observer and High-frequency Injection and Dead-Time Compensation Scheme for Sensorless Vector Control System of PMSM," *2019 22nd International Conference on Electrical Machines and Systems (ICEMS)*, 2019, pp. 1-6.

[23] M. Seilmeier and B. Piepenbreier, "Sensorless Control of PMSM for the Whole Speed Range Using Two-Degree-of-Freedom Current Control and HF Test Current Injection for Low-Speed Range," *IEEE Transactions on Power Electronics*, vol. 30, no. 8, pp. 4394-4403, 2015.

[24] K. Yu, Y. Fan, J. Chen and Y. Wang, "Fault-Tolerant Sensorless Control of Position Sensor Failure for Permanent Magnet Vernier Machine," *2020 23rd International Conference on Electrical Machines and Systems (ICEMS)*, 2020, pp. 1251-1256.

[25] J. M. Liu and Z. Q. Zhu, "Improved Sensorless Control of Permanent-Magnet Synchronous Machine Based on Third-

Harmonic Back EMF," in *IEEE Transactions on Industry Applications*, vol. 50, no. 3, pp. 1861-1870, 2014.
[26] X. Song, B. Han, S. Zheng and S. Chen, "A Novel Sensorless Rotor Position Detection Method for High-Speed Surface PM Motors in a Wide Speed Range," *IEEE Transactions on Power Electronics*, vol. 33, no. 8, pp. 7083-7093, 2018.
[27] B. WANG, C. LIU and J. SHANG, "Sensorless Control of Permanent Magnet Synchronous Motor Based on Extended State Observer," *2019 22nd International Conference on Electrical Machines and Systems (ICEMS)*, 2019, pp. 1-5.
[28] A. Eilenberger and M. Schroedl, "Extended back EMF model for PM synchronous machines with different inductances in d- and q-axis," *2008 13th International Power Electronics and Motion Control Conference*, 2008, pp. 945-948.
[29] J. M. Liu and Z. Q. Zhu, "Improved Sensorless Control of Permanent-Magnet Synchronous Machine Based on Third-Harmonic Back EMF," *IEEE Transactions on Industry Applications*, vol. 50, no. 3, pp. 1861-1870, 2014.
[30] T. Wang *et al*., "An EMF Observer for PMSM Sensorless Drives Adaptive to Stator Resistance and Rotor Flux Linkage," *IEEE Journal of Emerging and Selected Topics in Power Electronics*, vol. 7, no. 3, pp. 1899-1913, 2019.
[31] N. K. Quang, N. T. Hieu and Q. P. Ha, "FPGA-Based Sensorless PMSM Speed Control Using Reduced-Order Extended Kalman Filters," *IEEE Transactions on Industrial Electronics*, vol. 61, no. 12, pp. 6574-6582, 2014.
[32] Z. Wang, Y. Zheng, Z. Zou and M. Cheng, "Position Sensorless Control of Interleaved CSI Fed PMSM Drive With Extended Kalman Filter," in *IEEE Transactions on Magnetics*, vol. 48, no. 11, pp. 3688-3691, 2012.
[33] P. Borsje, T. F. Chan, Y. K. Wong and S. L. Ho, "A Comparative Study of Kalman Filtering for Sensorless Control of a Permanent-Magnet Synchronous Motor Drive," *IEEE International Conference on Electric Machines and Drives, 2005.*, 2005, pp. 815-822.
[34] E. Laroche, E. Sedda and C. Durieu, "Methodological Insights for Online Estimation of Induction Motor Parameters," in *IEEE Transactions on Control Systems Technology*, vol. 16, no. 5, pp. 1021-1028, 2008.
[35] K. Liu and Z. Q. Zhu, "Position-Offset-Based Parameter Estimation Using the Adaline NN for Condition Monitoring of Permanent-Magnet Synchronous Machines," in *IEEE Transactions on Industrial Electronics*, vol. 62, no. 4, pp. 2372-2383, 2015.
[36] T. D. Batzel and K. Y. Lee, "An approach to sensorless operation of the permanent-magnet synchronous motor using diagonally recurrent neural networks," in *IEEE Transactions on Energy Conversion*, vol. 18, no. 1, pp. 100-106, 2003.
[37] Q. An, J. Zhang, Q. An and A. Shamekov, "Quasi-Proportional-Resonant Controller Based Adaptive Position Observer for Sensorless Control of PMSM Drives Under Low Carrier Ratio," in *IEEE Transactions on Industrial Electronics*, vol. 67, no. 4, pp. 2564-2573, 2020.
[38] M. N. Uddin, H. Zou and F. Azevedo, "Online Loss-Minimization-Based Adaptive Flux Observer for Direct Torque and Flux Control of PMSM Drive," *IEEE Transactions on Industry Applications*, vol. 52, no. 1, pp. 425-431, 2016.
[39] T. D. Do, "Disturbance Observer-Based Fuzzy SMC of WECSs Without Wind Speed Measurement," *IEEE Access*, vol. 5, pp. 147-155, 2017.
[40] A. A. Alfehaid, E. G. Strangas and H. K. Khalil, "Sensorless Speed Control of PMSM Using Extended High-Gain Observers," *2019 American Control Conference (ACC)*, 2019, pp. 2576-2581.
[41] M. A. Mossa, "Effective predictive current control for a sensorless five-phase induction motor drive," *Int. J. Power Electron*., vol. 13, pp. 502–532, 2021.
[42] W. Lu *et al*., "New Sensorless Vector Control System With High Load Capacity Based on Improved SMO and Improved FOO," *IEEE Access*, vol. 9, pp. 40716-40727, 2021.
[43] M. A. Mossa, H. Echeikh, A. Iqbal, T. Duc Do, A. S. Al-Sumaiti, "A Novel Sensorless Control for Multiphase Induction Motor Drives Based on Singularly Perturbed Sliding Mode Observer-Experimental Validation," *Appl. Sci*., vol. 10, p. 2776, 2020.
[44] Y. Zhu, M. Cheng, W. Hua and B. Zhang, "Sensorless Control Strategy of Electrical Variable Transmission Machines for Wind Energy Conversion Systems," *IEEE Transactions on Magnetics*, vol. 49, no. 7, pp. 3383-3386, 2013.
[45] A Khlaief, M. Boussak, A. Châari, "A MRAS-based stator resistance and speed estimation for sensorless vector controlled IPMSM drive," *Electric Power Systems Research*, vol. 108, 2014, pp. 1-15.
[46] K. Saad, K. Abdellah, H. Ahmed, and A. Iqbal, "Investigation on SVM-Backstepping sensorless control of five-phase open-end winding induction motor based on model reference adaptive system and parameter estimation," *Engineering Science and Technology, an International Journal*, vol. 22, no. 4, pp. 1013-1026, 2019.
[47] S. Khadar, H. Abu-Rub and A. Kouzou, "Sensorless Field-Oriented Control for Open-End Winding Five-Phase Induction Motor With Parameters Estimation," in *IEEE Open Journal of the Industrial Electronics Society*, vol. 2, pp. 266-279, 2021.
[48] D. Semenov, B. Tian, Q. An and L. Sun, "Position estimation for sensorless FOC of five-phase PMSM in electric vehicles," *2016 Australasian Universities Power Engineering Conference (AUPEC)*, 2016, pp. 1-5.
[49] H. Echeikh, R. Trabelsi, A. Iqbal, M. Mimouni, "Real time implementation of indirect rotor flux oriented control of a five-phase induction motor with novel rotor resistance adaption using sliding mode observer," *Journal of the Franklin Institute*, vol. 355, no. 5, pp. 2112-2141, 2018.
[50] M. R. Khan and A. Iqbal, "Extended Kalman filter based speeds estimation of series-connected five-phase two-motor drive system." *Simul. Model. Pract. Theory*, vol. 17, pp. 1346-1360, 2009.
[51] H. Abu-Rub, M. R. Khan, A. Iqbal and S. M. Ahmed, "MRAS-based sensorless control of a five-phase induction motor drive with a predictive adaptive model," *2010 IEEE International Symposium on Industrial Electronics*, 2010, pp. 3089-3094.
[52] D. Semenov, B. Tian, Q. An and L. Sun, "Position estimation for sensorless FOC of five-phase PMSM in electric vehicles," *2016 Australasian Universities Power Engineering Conference (AUPEC)*, 2016, pp. 1-5
[53] N. Bounasla, S. Barkat, E. Benyoussef and K. Tounsi, "Sensorless sliding mode control of a five-phase PMSM using extended Kalman filter," *2016 8th International Conference on Modelling, Identification and Control (ICMIC)*, 2016, pp. 97-102
[54] T. Michalski, C. Lopez, A. Garcia and L. Romeral, "Sensorless control of five phase PMSM based on extended Kalman filter," *IECON 2016 - 42nd Annual Conference of the IEEE Industrial Electronics Society*, 2016, pp. 2904-2909.
[55] B. Tian, M. Molinas, Q. An, B. Zhou and J. Wei, "Freewheeling current-based sensorless field-oriented control of Five-Phase PMSMs under IGBT failures of a single phase," *IEEE Transactions on Industrial Electronics*, vol. 69, no. 1, pp. 213-224, 2021.
[56] A. Hezzi, M. N. Abdelkrim and S. B. Elghali, "Sensorless Backstepping Drive for a Five-Phase PMSM based on Unknown Input Observer," *2020 20th International Conference on Sciences and Techniques of Automatic Control and Computer Engineering (STA)*, 2020, pp. 125-130.
[57] N. K. Nguyen, E. Semail, F. De Belie and X. Kestelyn, "Adaline Neural Networks-based sensorless control of five-phase PMSM drives," *IECON 2016 - 42nd Annual Conference of the IEEE Industrial Electronics Society*, 2016, pp. 5741-5746.
[58] H. Chen, C. Hsu and D. Chang, "Position sensorless control for five-phase permanent-magnet synchronous motors," *2014 IEEE/ASME International Conference on Advanced Intelligent Mechatronics*, 2014, pp. 794-799.
[59] A. Lokriti, Y. Zidani, and S. Doubabi, "Comparaison des performances des régulateurs PI et IP appliques pour la

commande vectorielle a flux rotorique orienté d'une machine asynchrone," *Proceedings of the 8th international IFAC conference on modeling & simulation MOSIM*, 2010, pp. 1–7.

[60] M. S. Mahmoud, A. Alameer and M. M. Hamdan," An adaptive sliding mode control for single machine infinite bus system under unknown uncertainties," *International Journal of Robotics and Control Systems*, vol. 1, no. 3, pp. 226-243, 2021.

[61] M. S. Mahmoud, R. A. Saleh and A. Ma'arif, "Stabilizing of inverted pendulum system using Robust sliding mode control," *International Journal of Robotics and Control Systems*, vol. 2, no. 2, pp. 230-239, 2022.

[62] Y. Zahraoui, M. Akherraz and A. Ma'arif, "A Comparative Study of Nonlinear Control Schemes for Induction Motor Operation Improvement," *International Journal of Robotics and Control Systems*, vol. 2, no. 1, pp. 1–17, 2022.

[63] Y. D. Landau, "Adaptive control: The model reference approach," in *IEEE Transactions on Systems, Man, and Cybernetics*, vol. SMC-14, no. 1, pp. 169-170, Jan.-Feb. 1984.

[64] I. Landau, "A hyperstability criterion for model reference adaptive control systems," *IEEE Transactions on Automatic Control*, vol. 14, no. 5, pp. 552-555, 1969.

[65] W. T. Asfu, "Stator Current-Based Model Reference Adaptive Control for Sensorless Speed Control of the Induction Motor," *Journal of control science and Engineering*, vol. 2020, p. 8954704, 2020.

[66] R. Ortega, L. Praly and I. Landau, "Robustness of discrete-time direct adaptive controllers," in *IEEE Transactions on Automatic Control*, vol. 30, no. 12, pp. 1179-1187, 1985

[67] L. Dugard, I. Landau and H. Silveira, "Adaptive state estimation using MRAS techniques--Convergence analysis and evaluation," in *IEEE Transactions on Automatic Control*, vol. 25, no. 6, pp. 1169-1182, 1980.